Journal of Membrane Science 624 (2021) 119103

Contents lists available at ScienceDirect

Journal of Membrane Science

journal homepage: http://www.elsevier.com/locate/memsci

Techno-economic assessment of postcombustion carbon capture using high-performance nanoporous single-layer graphene membranes

M. Micari, M. Dakhchoune, K.V. Agrawal *

Laboratory of Advanced Separations (LAS), Ecole Polytechnique Federale de Lausanne (EPFL), Sion, Switzerland

ARTICLE INFO

Keywords:
Postcombustion carbon capture
Nanoporous single-layer graphene membranes
Techno-economic feasibility
Gas separation
Membrane process

ABSTRACT

High-performance membranes have emerged as an energy-efficient alternative to absorption-based postcombustion carbon capture. So far, the techno-economic analyses have been centered around the polymeric membranes. Recently, nanoporous single-layer graphene (NSLG) membranes have yielded large CO_2 permeance, making them attractive for capture. Herein, we assess the techno-economic feasibility of NSLG-based capture using an optimized process. The most suitable system to achieve recovery and purity of 90% comprises a double-stage process with (i) recycle of 2nd stage retentate, and (ii) multi-staged vacuum pumps for the permeate, including roots pumps in series with liquid-ring pumps and intermittent condensers for water vapor. The high CO_2 permeance of NSLG makes the vacuum process without feed compression more economically competitive, even if the area required is higher. Attractive capture penalties are estimated despite a conservative membrane cost (500 \$/m^2): 41.2 and 31.8 \$/ton$_{CO2}$ from wet feeds with CO_2 concentration of 10% and 13.5%, respectively, corresponding to energy penalty of 1.53 and 1.24 MJ/kg$_{CO2}$. For steel and cement industries where CO_2 concentration is favorably high (25%) but electricity cost is also higher (0.10–0.20 \$/kWh), the capture penalty ranges from 28.0 to 46.0 \$/ton$_{CO2}$. Overall, the analysis shows that NSLG membranes are competitive with state-of-the-art processes for postcombustion capture.

1. Introduction

The rise of CO_2 emissions due to the intensification of the industrial sector has led to increasing concerns over global warming [1]. The mitigation pathways proposed by the Intergovernmental Panel on Climate Change (IPCC) to limit warming to 1.5 °C, as required by the Paris Agreement, strive for net-zero CO_2 emissions by 2050 [2]. To reduce the emissions from the fossil-fuel-dependent processes, several approaches for carbon capture, utilization, and storage (CCUS) have been proposed. Carbon capture can be categorized in (i) precombustion capture from the mixture obtained from reforming of fossil fuels; (ii) oxycombustion capture involving separation of oxygen from the air used for combustion, and (iii) postcombustion capture of CO_2 from the flue gas produced by power plants, steel and cement industries, etc. [3]. Precombustion and oxycombustion capture routes are more attractive for new power plants because they require a significant redesign of the plant. In contrast, postcombustion capture is a promising approach to reduce the emissions of existing plants by retrofitting the capture unit. One can also implement it on a decentralized basis for small-scale emission sources. For this reason, many studies have focused on the development and optimization of capture processes for postcombustion CO_2 capture. Currently, the most mature technology for postcombustion capture is based on the chemisorption of CO_2 (with amines such as monoethanolamine) [4,5]. At the moment, 19 large-scale plants with CCS facilities are operational worldwide and have a total capture capacity of 39 million tons of CO_2 per year [6]. While absorption-based technology has been demonstrated at the large-scale, it involves a large capture penalty (48–111 \$/ton$_{CO2}$ [7]) and large energy requirements, mainly arising from the thermal energy needed to strip the absorbed CO_2 and to regenerate the solvent (from 3 to 4 MJ/kg$_{CO2}$) [3,8]. Furthermore, the amines are not environmental-friendly. Their implementation on a decentralized basis is expected to be challenging due to a high cost of maintenance and supply/disposal of the solvent. Therefore, to overcome these limitations, high-performance membrane-based separation processes are being intensively investigated [9]. Membrane processes have a lower environmental impact than amines because they neither consume chemicals nor generate waste [4,8].

The targets of purity and recovery of CO_2 from flue gas are very

* Corresponding author.
E-mail address: kumar.agrawal@epfl.ch (K.V. Agrawal).

https://doi.org/10.1016/j.memsci.2021.119103
Received 8 October 2020; Received in revised form 15 January 2021; Accepted 19 January 2021
Available online 26 January 2021

stringent, typically higher than 90%, to ensure a significant reduction in the emissions and to minimize the subsequent costs for compression and transport [10]. This is challenging to obtain from a single-stage membrane process because the CO_2 concentration in flue gas is small (10–20%). Therefore, it becomes unavoidable to implement a multi-stage membrane configuration [11]. Double-stage membrane process has been reported as the most suitable configuration to meet the targets [10,11]. Several studies on the techno-economic analysis of such process used compressors to increase the feed pressure or vacuum to reduce the permeate pressure, to generate a driving force for CO_2 diffusion [10,12]. Typically, representative parameters, such as specific area [$m^2/(kg_{CO2}/s)$], specific energy [MJ/kg_{CO2}], and CO_2 capture penalty [$\$/ton_{CO2}$], are reported for chosen operating conditions (feed and permeate pressures), membrane properties (CO_2 permeance, selectivity, membrane lifespan) and associated costs (energy cost as well as the capital cost for membranes, pumps, compressors, etc.).

Favre reported the key challenges of the application of membranes for postcombustion capture and identified the ranges of operating conditions where the membrane process can be competitive with the state-of-art absorption process [3]. In particular, he reported that the membrane process with feed compression can be competitive only when the inlet CO_2 concentration is higher than 20%, because of the high energy consumption of the compression step. Conversely, with the vacuum in the permeate side, the membrane process was reported to consume lower energy but needed a larger area, thus, he predicted that lower cost- or higher productivity-membranes will be required to make the process competitive. In agreement with these findings, Yang et al. reported that a double-stage membrane process, with feed compression and with recycle of the retentate from the second stage, can be competitive with the amine process. They reported specific capture costs in the range of 45–80 $\$/ton_{CO2}$ [10]. The process using vacuum pumps was reported to be more expensive because of the higher capital costs of such pumps and because of the higher membrane area required. At the same time, Merkel et al. demonstrated the economic feasibility of a double-stage membrane process with a combination of feed compression (2 bar) and vacuum in permeate (0.2 bar), resulting in a specific cost of 39 $\$/ton_{CO2}$. Furthermore, they showed that the employment of counter-flow membrane modules with a sweep in the permeate channel made the system more feasible, as the specific cost reduced to 23 $\$/ton_{CO2}$. Counter-flow modules maximize the driving force in the whole membrane length, therefore, the membrane area required as well as the power consumption are lower than those with cross-flow modules, for the same targets [12]. On the other hand, cross-flow modules have a number of advantages: (i) lower geometrical complexity, (ii) limited pressure drops and (iii) low concentration polarization in the permeate channel [13]. Finally, Merkel et al. found that the capture penalty is not affected significantly by an increase of CO_2/N_2 selectivity beyond 30 [12]. Conversely, the CO_2 permeance was shown to have much more impact on the required membrane area and the cost, a finding that was also confirmed by Zhao et al. [4].

Concerning the economic parameters, Ramasubramanian et al. investigated the impact of membrane and energy costs on the capture penalty from a double-stage process with a vacuum of 0.2 bar in the permeate, ambient pressure in the feed, and a recycle stream [1]. Using CO_2 permeance of 3000 GPU, the minimum CO_2/N_2 selectivity required to achieve recovery of 90% and purity of 95% was reported to be 160. The corresponding capture penalty was in the range of 20–30 $\$/ton_{CO2}$.

Roussanaly et al. performed a benchmarking of the needed membrane selectivity and CO_2 permeance to make the membrane process competitive with the absorption [9]. They identified regions within the possible membrane performance range where simple membrane process configurations as well as more advanced configurations, including recycle or sweep, are competitive with the absorption technology. They found that simple membrane process configurations are competitive when selectivity is higher than 65 and permeance is higher than 1100 GPU, whereas more advanced configurations are competitive even when selectivity is around 30 with high permeance or when permeance is around 370 GPU with high selectivity. Finally, the comparison of such regions with the properties of several current or under development membranes highlighted the importance to produce a very thin selective layer.

Within the context of the optimal process design, Gabrielli et al. developed an optimization framework to find membrane configurations minimizing energy consumption and membrane area. They found that the double-stage configuration with the recycle of the retentate from the second stage is the most suitable to achieve high purity and recovery targets. Moreover, the sensitivity analysis of the number of membrane stages highlighted that the increase in the number of stages always leads to an increase of membrane area. Conversely, the energy consumption showed a global minimum with three membrane stages. A further increase in the number of stages caused an increase in the membrane area as well as the energy consumption [14].

Furthermore, several reports have proposed superstructure-based optimization methods to identify the optimal membrane process configuration for the separations of various gas mixtures [15,16]. Concerning the separation of flue gas from power plants, Arias et al. proposed a nonlinear programming optimization approach to find the optimal configuration for a wide range of target CO_2 purity [17]. They found that (i) for purity ranging from 90 to 93%, the optimal system is based on two stages with recycle of the 2nd retentate, (ii) for purity ranging from 94 to 96%, the optimal system is based on three stages and two recycles (retentate and the permeate of the last stage), and (iii) for purity higher than 97%, four stages (i.e., the maximum number of stages considered) are needed. A similar approach with wider ranges of variables and configurations has been proposed by Mores et al. [18]. They found that a four-stage configuration with feed compression and permeate vacuum is optimal to achieve 95% recovery and 98% purity of CO_2. The optimal number of stages depended on the purity, as already showed by Arias et al., but not on the recovery. Also, they demonstrated that lower number of stages are required for the same targets when the CO_2 permeance of the membranes increases. The impact of the membrane properties was also investigated by Lee et al., who implemented a genetic algorithm optimization method to obtain optimal solutions among all the practically feasible networks [19]. They demonstrated that increasing the CO_2 permeance and CO_2/N_2 selectivity up to 4000 GPU and 50, respectively, leads to a significant decrease of the CO_2 capture cost with the two-stage membrane system. Also, they showed that it is favorable to employ membranes with high CO_2 permeance in the first stage and membranes with high CO_2/N_2 selectivity in the second stage to reduce electricity consumption and achieve high purity. A similar finding was reported by Xu et al., who proposed a systematic analysis of the impact of the feed pressure and membrane selectivity on the required membrane area, energy consumption, and capture penalty. They considered a double-stage membrane system with feed compression and recycle. They showed that the employment of high permeance-membranes in the first stage and of high selectivity-membranes in the second allows for reducing membrane area and electricity consumption, even taking into account the constrain on membranes' performance given by the Robeson curve [11].

So far, the techno-economic analyses for membrane-based post-combustion carbon capture have been based on polymeric membranes, which have processability and scalability advantages over the inorganic membranes. In particular, the membranes based on polymer thin selective layers hosting CO_2-selective groups (ether, amines) have yielded high performance. One of the most promising membrane materials is polyethylene oxide (PEO), rich in polar groups, which create a high affinity to CO_2. However, high-molecular-weight PEO tends to crystallize and this reduces the membrane performance [20]. To avoid this, PEO is often modified. Modified PEO-based membranes such as Polaris™ developed by Membrane Technology and Research, Inch. and the PolyActive™ by GKSS Research Center have shown attractive performance [21]. Polaris™ membranes have achieved a CO_2/N_2

selectivity of 49 and CO_2 permeance of 2000 GPU [22].

Furthermore, facilitated-transport membranes have been developed by incorporating amine groups inside the polymer matrix. The membranes prepared using polyvinyl alcohol and polyvinylamine have resulted in large CO_2/N_2 selectivity, up to 170 [21,23]. Recently, hybrid materials such as metal-induced microporous polymers (MMPs) have yielded attractive performance. MMPs allow selective, reversible sorption of CO_2, enhancing the transport of CO_2 through coated substrates. They have good hydrolytic stability and resulted in promising capture performance with CO_2 permeance of 3000 GPU and CO_2/N_2 selectivity of 78 [24].

A promising way to further improve the prospect of carbon capture is to increase CO_2 permeance while maintaining a moderate selectivity (>20). In this respect, membranes hosting an extremely thin selective layer, such as those based on nanoporous single-layer graphene (NSLG) are especially promising. A molecular simulation study from Liu et al. demonstrated the suitability of nitrogen-functionalized NSLG for CO_2/N_2 separation where CO_2 permeance in the order of 10^5 GPU and CO_2/N_2 selectivity of around 300 were predicted with a pore density of 4×10^{12} cm^{-2} and pore size of ~3.4 Å [25]. Another simulation by Tian et al. showed that decorating NSLG with ionic liquid can lead to the ion-gating effect, which results in a highly selective CO_2 transport with permeance reaching 10^5 GPU [26]. Our group recently demonstrated a proof-of-principle for polymer-functionalized NSLG, which yielded an attractive combination of CO_2 permeance (6180 GPU) and CO_2/N_2 selectivity (22.5) [27]. Recent improvement of this route has further pushed the performance with CO_2 permeance of 10000 GPU and CO_2/N_2 selectivity over 30 (unpublished data). Furthermore, significant technological advances in the past few years have led to the industrial-scale production of the graphene films. In the last five years, the global production capacity of graphene films has sharply increased and has shown to be economically scalable [28]. In addition, the etching techniques to improve the membrane performance have been recently proven by our group to be highly scalable [52]. Attributing to the fact that these are relatively new developments, so far, there is no study on the design of an economically-viable capture process using the NSLG membranes. Therefore, there is a need to assess if the separation process based on NSLG membranes can be economically-feasible.

Furthermore, much attention has been paid on the optimization of the operating conditions when feed compression is implemented, while it has been found that systems with vacuum in the permeate channels are generally less economically feasible because of the high membrane area needed in the latter case [4,10]. However, generally speaking, the economic feasibility depends on a trade-off between capital costs, driven by the required membrane area, and operating costs, mostly given by the electricity consumption [14]. Therefore, vacuum operations or combinations of vacuum and compression may be promising options in various scenarios, where the reduction of operating costs leads to lower capture cost even when the capital cost increases [18,29]. Since a systematic investigation of the impact of vacuum permeate pressures on energy consumption and membrane area in the presence of highly permeable membranes is missing, this work aims at assessing as to which operating conditions can minimize the capture penalty with NSLG membranes.

Herein, we report a systematic analysis of the most suitable process layouts and operating conditions for efficient postcombustion capture based on high-performance NSLG membranes. Such processes are particularly attractive for decentralized purification systems and for small-to medium-scale CO_2 capture plants, e.g., community-scale boilers. We simulate various system layouts (with feed compression or with permeate vacuum, double-stage without and with recycle) to find the optimal configuration. Then, we find the optimal operating conditions, in terms of feed and permeate pressure as well as membrane area, which are required to achieve the purity and recovery targets while minimizing the CO_2 capture penalty from dry and wet feeds with variable CO_2 concentration (10–14% from the power plant; 20–25% from the steel and cement industry). We show that carbon capture with the high-performance membranes is highly competitive even with a conservative membrane cost of 500 $/m^2. On the basis of per ton of captured CO_2, the capture penalty reduces from $41.2 to $31.8 when the feed CO_2 concentration increases from 10 to 13.5% and the energy need reduces from 1.53 to 1.24 MJ/kg_{CO2}. Owing to the high CO_2 permeance (10000 GPU), the needed membrane area to capture 0.5 million ton of CO_2 on an annual basis is relatively low (2904 and 1995 $m^2/(kg_{CO2}/s)$ for inlet CO_2 concentrations of 10 and 13.5%, respectively). Finally, from the steel and cement industry, where the CO_2 concentration is 25% but the energy cost is higher (0.10–0.20 $/kWh as against 0.05 $/kWh in the case of power plants), the capture penalty turns out to be comprised between 28.0 and 46.0 $/$ton_{CO2}$. Overall, we demonstrate that economically-viable CO_2 capture is indeed possible based on the high-performance NSLG membranes.

2. Methods

This section presents the fundamental equations of the technical model describing (i) the single stage, (ii) the double stage, and (iii) the double stage with recycle. Subsequently, models to estimate the energy consumption of the vacuum pumps and the compressors included in the configurations are discussed. Finally, an economic model comprising of operating and capital costs is presented.

2.1. Modeling single-stage process

The driving force for the transport of gaseous species through the membrane is the chemical potential difference between the feed and the permeate side. This difference corresponds to a partial pressure gradient, generated either via feed compression or via vacuum in the permeate. The model used to estimate the transmembrane flux of each component of the gas mixture and to calculate the profiles of concentration and flow rates on the feed and permeate side is adapted from the previous models reported in the literature [13,30]. The membrane length (along the z-axis) is discretized, and in each discretization element z^{th}, the *trans*-membrane fluxes are calculated (Fig. 1).

A cross-plug flow is assumed, thus the concentration on the feed side changes from one element to the following whereas the transmembrane flux is collected immediately after crossing the membrane and then mixed with the fluxes arriving from the previous elements, to generate the outlet permeate stream. This means that no mixing is supposed to occur along the permeate channel. The other main assumptions of the model are the following: (i) the permeance of the components is independent of the pressure; (ii) the pressure drops in both sides are negligible; (iii) the process is isothermal; (iv) concentration polarization is negligible.

For each discretization element z^{th}, the flux (J_i [mol/(m^2s)]) of the component *i* is expressed as a function of its permeance ($\mathbf{P}_i$ [mol/(m^2sPa)]) through the membrane and the difference of its partial

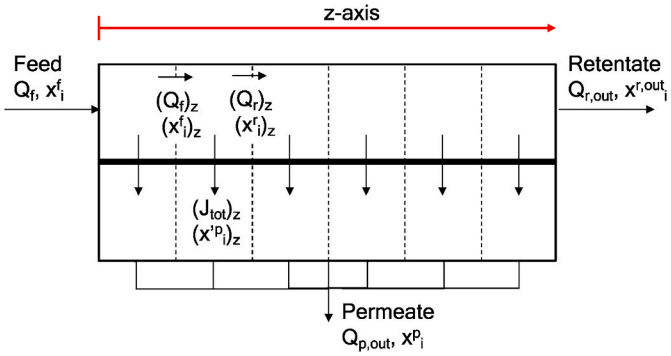

Fig. 1. Schematic representation of a single stage with cross-plug flow arrangement.

pressures at the two sides of the membrane (Eq. (1)).

$$J_i = \boldsymbol{P}_i\left(P_i^f - P_i^{'p}\right) = \boldsymbol{P}_i\left(P_{feed}x_i^f - P_{perm}x_i^{'p}\right) \quad (1)$$

It is worth noting that the difference of the partial pressures is between the one at the bulk of the feed side (P_i^f [Pa]) and the one on the permeate side right after the selective membrane film ($P_i^{'p}$ [Pa]). In fact, since no mixing is supposed to occur along the permeate channel because of the cross-plug flow assumption (which means that $(x_i^{'p})_z \neq x_i^p$), the flux is dependent on the variation of the concentration in the feed side but not on the one of the mixed permeate stream [14].

The total transmembrane flux is given by the sum of the fluxes of the components and each flux is related to the total flux through the fraction of the component in the permeate side close to the membrane, as reported in equations (2) and (3).

$$J_{tot} = \sum_i J_i \quad (2)$$

$$J_i = x_i^{'p} J_{tot} \quad (3)$$

The system of equations reported above presents *(2i+1)* equations and can be solved iteratively to calculate the fluxes and the concentrations $x_i^{'p}$ for each component and the total flux for each membrane discretization element.

The fluxes are then used to calculate the flow rate (Q_r [mol/s]) and concentration (x_i^r [−]) of the retentate of the discretization element, which corresponds to the feed of the following element. Equations (4) and (5) report, for a generic discretization element z^{th}, the total mass balance and the mass balance on component *i* on the feed side.

$$\left(Q_f\right)_z = \left(Q_r\right)_z + \left(J_{tot}dA\right)_z \quad (4)$$

$$\left(Q_f x_i^f\right)_z = \left(Q_r x_i^r\right)_z + \left(J_i dA\right)_z \quad (5)$$

Finally, the permeates produced in each discretization element are collected to generate the outlet permeate, whose concentrations (x_i^p [−]) and flow rate ($Q_{p,out}$ [mol/s]) are estimated according to equations (6) and (7).

$$Q_{p,out} = \sum_z \left(J_{tot}dA\right)_z \quad (6)$$

$$Q_{p,out}x_i^p = \sum_z \left(J_i dA\right)_z \quad (7)$$

When the available membrane area and the pressures in the feed and in the permeate channels are given, the above equations are used to simulate a single stage with cross-flow configuration. When only the pressures are given, the model is able to design a suitable single stage, via an optimization algorithm that calculates the membrane area required to achieve a certain separation. The algorithm minimizes the sum of the quadratic errors between the calculated and target recovery and purity.

2.2. Modeling of double stage

In most cases, a single stage is not sufficient to achieve the given targets of purity and recovery. Therefore, two stages can be combined in a stripper cascade or in an enricher cascade: in the first case, the retentate exiting the first stage is fed to the second stage, whereas, in the second case, the permeate produced by the first stage is sent to the second. In this work, we considered only the enricher cascade, since the aim of the process is to achieve high purity of the permeated component (CO_2). The double-stage with enricher configuration and with vacuum pumps for the permeate streams (instead of compressors for the feed streams) is represented in Fig. 2.

For the simulation of a double stage with given membrane areas and pressures, we simulate twice the single stage with the system of equations reported in paragraph 2.1 and we set the composition and flow rate of the feed of the second stage equal to the composition and flow rate of the permeate generated by the first stage. Also, in this case, an optimization algorithm has been implemented to identify the areas of the two membrane stages able to achieve the targets of purity and recovery for a given set of pressures. Furthermore, a higher-level minimization algorithm has been included to find the set of pressures minimizing the global cost. The procedure followed to design a double-stage system and to identify the operating conditions minimizing the global capture cost is sketched in Fig. 3.

2.3. Modeling of double stage with recycle

In order to increase the recovery, many works showed that the best configuration is a double-stage with the recycle of the retentate stream exiting the second unit. In fact, the CO_2 concentration in the 2nd retentate is relatively high, and by recycling this stream, the overall CO_2 recovery, as well as the driving force in the first membrane stage, increases. To simulate such configuration, we implemented a model for the double-stage with recycle, which consists of solving a double-stage iteratively while varying the feed entering the first stage until the difference between the guess and the calculated outlet retentate flow rate and composition is higher than a given tolerance. In this regard, the flow rate (Q_f^* [mol/s]) and the composition (x_i^{f*} [−]) of the feed entering the first stage are given in equations (8) and (9).

$$Q_f^* = Q_f + Q_{r,out2} \quad (8)$$

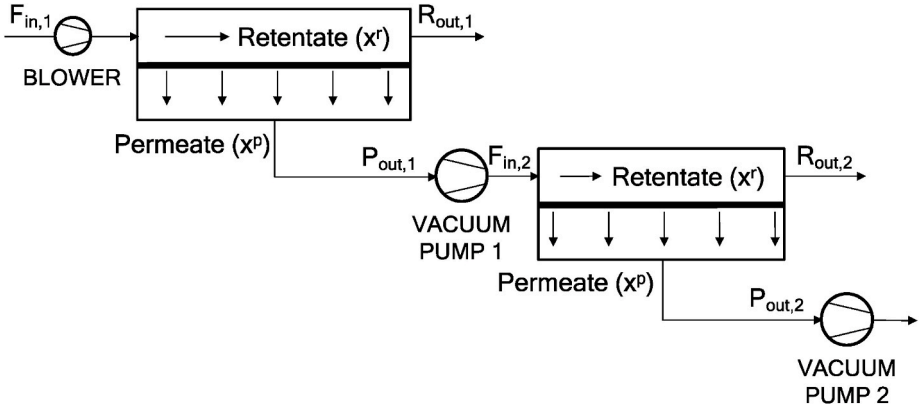

Fig. 2. Sketch of the double stage where the two stages are combined in an enricher cascade and the driving force is realized by using vacuum pumps in the permeate.

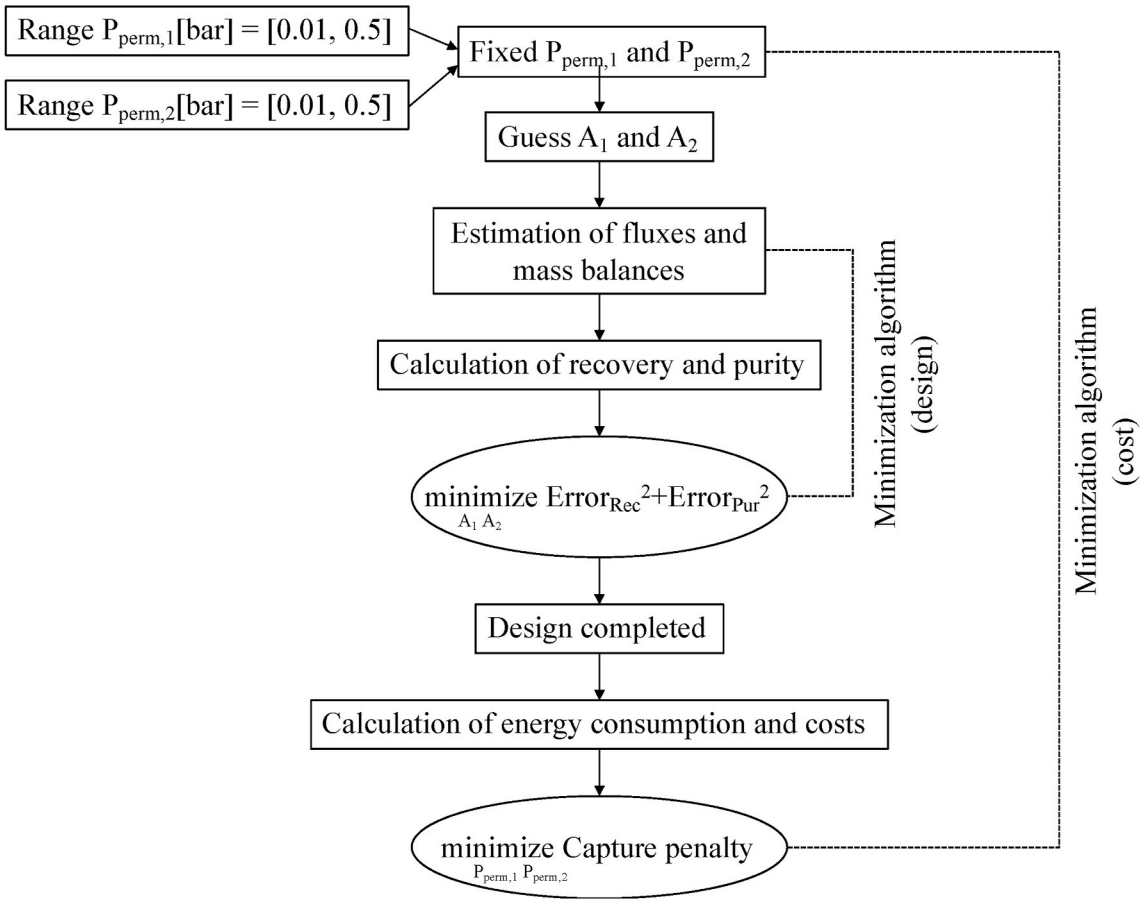

Fig. 3. The procedure for optimizing the design of a double-stage process able to achieve the separation targets. The minimization algorithm (design) minimizes the error between the calculated and the target purity and recovery to find the required areas. The minimization algorithm (cost) identifies the pressures corresponding to the minimum capture penalty.

$$Q_f^* x_i^{f*} = Q_f x_i^f + Q_{r,out2} x_i^{r,out2} \tag{9}$$

The double-stage configuration with recycle of the 2nd retentate is reported in Fig. 4. In the layout reported for the double-stage with recycle, as in the one for the double stage, the pressure difference is realized through vacuum pumps for the permeate streams.

In analogy with the model of the double-stage, a minimization algorithm has been implemented to estimate the membrane areas required with a double-stage system with recycle to achieve certain targets of purity and recovery. In addition, a high-level minimization algorithm has been employed to find the set of pressures from a given range corresponding to the minimum capture penalty (as in Fig. 3 for the double stage).

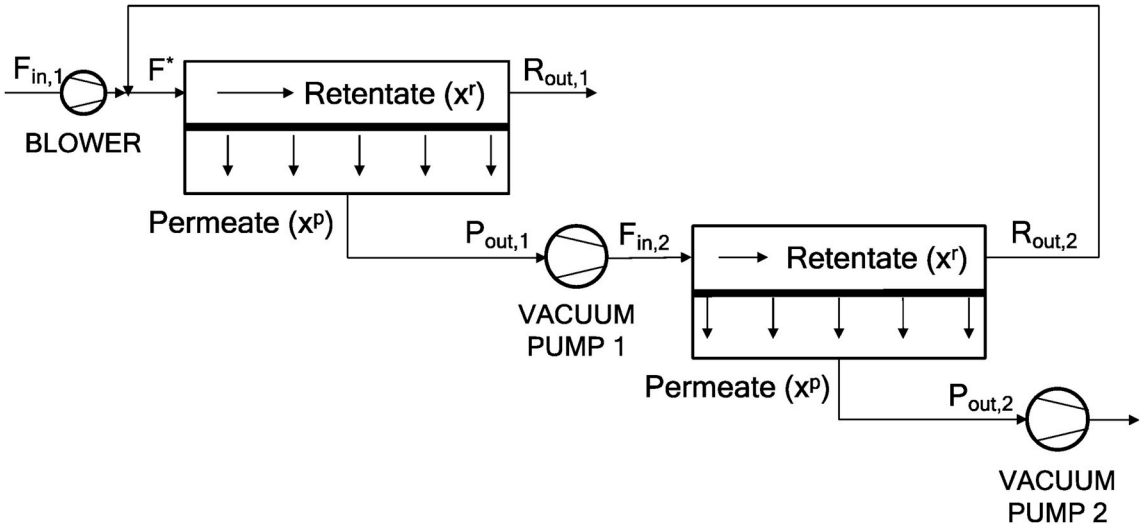

Fig. 4. Sketch of the double stage with recycle of the retentate produced by the 2nd stage, and with vacuum pumps for the permeate streams.

2.4. Definition of recovery and purity

For any simulated configuration, crucial output values are recovery and purity, calculated with reference to CO_2. The recovery is defined as the ratio between the flow rate of CO_2 in the outlet permeate and the flow rate of CO_2 in the feed stream (equation (10)).

$$R_{CO2} = \frac{Q_{p,out} x^{p}_{CO2}}{Q_f x^{f}_{CO2}} \tag{10}$$

The purity is defined as the concentration of CO_2 in the outlet permeate. In the case of wet feed, the purity is always defined on a dry basis, as in equation (11) [11].

$$P_{CO2} = \frac{x^{p}_{CO2}}{1 - x^{p}_{H2O}} \tag{11}$$

2.5. Estimation of the energy consumption

The energy requirement of the membrane-based separation process is given by the energy requirement of the compressors and the vacuum pumps. Here, we compare the capture cost of configurations which use either feed compressor or vacuum in the permeate. The power consumption of the compressor, P_{compr} [W], can be expressed using the adiabatic compression term divided by an efficiency factor (equation (12)) [14].

$$P_{compr} = \frac{Q_{in,compr}}{\eta_{compr}} \frac{\gamma}{\gamma - 1} RT \left[\left(\frac{P_{high}}{P_{low}} \right)^{\frac{\gamma-1}{\gamma}} - 1 \right] \tag{12}$$

where $Q_{in,compr}$ [mol/s] is the flow rate entering the compressor, η_{compr} [−] is the efficiency of the compressor, γ [−] is the adiabatic index given by the combination of the indexes of the single gaseous components, P_{high} [bar] and P_{low} [bar] are the outlet and inlet pressures, respectively. This expression is also used to estimate the power consumption of the blower, included in the system configuration with vacuum pumps to pressurize the feed to 1.1 bar [12]. This slight increase of pressure is important to overcome any pressure drop that may occur along the membrane module.

For the vacuum pumps, we considered combinations of roots and liquid ring vacuum pumps (LRVP). More details about the selection of the pumps are given in paragraph 3.3. Roots pumps are designed for a small pressure increases (e.g. 0.07–0.10 bar), and the power required (P_{Roots} [W]) can be defined by modeling the compression as an isochoric process with a given efficiency, as reported in equation (13) [31].

$$P_{Roots} = \frac{Q^{vol}_{in,roots}}{\eta_{roots}} \left(P_{high} - P_{low} \right) \tag{13}$$

where $Q^{vol}_{in,\ roots}$ [m^3/s] is the volumetric flow rate entering the roots pump, η_{roots} [−] is the efficiency of the pump, P_{high} [bar] and P_{low} [bar] are the outlet and inlet pressures, respectively.

For LRVPs, the energy consumption can be expressed as that of an adiabatic transformation with a given efficiency (η_{LRVP} [−]), similarly to equation (12) [14]. The efficiency depends on the friction losses of the operating liquid and can be estimated knowing the geometry of the impeller, the properties of the fluid, and its speed [32].

2.6. Economic model

The economic model is composed of equations to estimate the capital and the operating costs of the membrane separation process. The capital costs include the cost of the membrane module (C_{membr} [US$]), and the cost of either compressors (C_{compr} [US$]) or the combination of vacuum pumps (C_{vacuum} [US$]) and the blower ($C_{blower}$ [US$]). The operating costs are given by the cost of the power required for the separation (C_{power} [US$/y]) and the cost for maintenance (C_{maint} [US$/y]). The capital costs are then annualized via a linear depreciation and by considering a lifetime of 25 years for pumps and compressors and of 5 years for the membranes [11]. The sum of annualized capital and operating costs divided by the amount of CO_2 recovered [ton/y] results in the specific CO_2 capture penalty [US$/$ton_{CO2}$] [33]. This representative economic output is used to compare the optimized membrane process with the state-of-art absorption technology, as well as with the polymeric membrane-based separation processes. The equations used to estimate the terms of costs are listed below (equations (14)–(19)).

$$C_{membr} = A_{membr,tot} \times C_{spec,m} \tag{14}$$

$$C_{compr} = Q_{in,compr} \times 0.0224 \times K_c \times 1.8 \tag{15}$$

$$C_{blower} = Q_{feed} \times 0.0224 \times K_c \times 1.8 \tag{16}$$

$$C_{vacuum} = C_{vacuum,ref} \left(\frac{Q_{in,vacuum}}{Q_{in,vacuumref}} \right)^{0.6} \tag{17}$$

$$C_{power} = P_{tot} \times 8000 \times C_{spec,power} \tag{18}$$

$$C_{maint} = 0.036 \times (C_{vacuum} + C_{blower}) + 0.01 \times C_{membr} \tag{19}$$

In equation (14), $A_{membr,tot}$ [m^2] is the total membrane area required, given by the sum of the areas of the two stages, and $C_{spec,m}$ [US$/$m^2$] is the specific cost of the membrane sheets. In equations (15) and (16), the parameter K_c [1/(m^3(STP)/s)] depends on the outlet pressure of the compressor: it is equal to 96,000 for pressures lower than 9 bar and 120,000 for pressures between 9 and 27 bar [10]. Equation (17) applies the widely used *six-tenths rule* to estimate the investment cost of the vacuum pumps starting from a reference point [34]. C_{vacuum}, given by equation (17), is the cost of a single vacuum pump with a design pumping speed at the inlet pressure equal to $Q_{in,vacuum}$ [m^3/h]. To estimate the total number of pumps in parallel, the total volumetric flow rate at the given pressure has to be divided by the design pumping speed. The reference points as well as the design pumping speeds for both roots pumps and LRVPs correspond to data given by the manufacturers. Further details are reported in paragraph 3.4 and in the supplementary materials. In equation (18), P_{tot} [W] is the total power, given by the sum of the power required either by vacuum pumps and blower or by the compressors; 8000 [h/y] is the number of annual operating hours [11]; and $C_{spec,power}$ [US$/kWh] is the specific cost of electricity. Finally, the maintenance cost in equation (19) is estimated as 3.6%/y of the investment cost of vacuum and blower (or of compressors) plus 1%/y of the membrane investment cost [4,10].

3. Description of the case studies

In this section, the inputs and parameters used for the simulation of case studies are presented and discussed.

3.1. Composition and flow rate of the flue gas

The separation process is designed to capture 0.5 million tons of CO_2 per year with recovery and purity of 90%. The case study makes reference to the real flue gas produced by a natural gas fired power plant where CO_2 concentration is around 11.8%. For a more conservative assessment, in the base case, we consider a molar concentration of CO_2 of 10%. This corresponds to an inlet total molar flow rate of the flue gas equal to 4385 mol/s (~384,310 m^3/h at ambient pressure). Later, we also compare capture penalties with higher concentrations of CO_2, taking multiple emission sources into account (from 10 to 14% for flue gas from power plants, 25% for flue gas from cement and steel plants). We perform simulations with both a dry feed and a wet feed saturated with water vapor at 50 °C (water vapor fraction of around 15% [11]). For the case of the dry feed, the inlet composition is: 10% CO_2 and 90% N_2. Conversely, for the case of the wet feed, the inlet composition is:

10% CO_2, 15% H_2O, 3% O_2 and 72% N_2. The other components of the flue gas such as NO_x and SO_x have not been accounted in the calculations since these can be almost completely removed in the pretreatment step [1,11].

3.2. Properties of the membranes

The membranes used for the simulations are based on NSLG functionalized with CO_2-selective groups [27]. The single-layer of graphene is mechanically-reinforced by a polymeric support. These membranes are characterized by high CO_2 permeance, thanks to an ultrathin selective layer, and a moderate CO_2/N_2 selectivity. In particular, the values used in our simulations are 10000 GPU for the CO_2 permeance and 30 for the CO_2/N_2 selectivity. These promising properties have been already realized in our laboratory. Further improvements of the membranes, including the increase of the selectivity by more sophisticated membrane functionalization processes, are expected in the near future. For the simulations with wet feed, the CO_2/H_2O and the CO_2/O_2 selectivity values are taken equal to 1 and 12.6, respectively, on the basis of experiments performed with NSLG membranes in our lab.

The graphene membrane module will likely be based on plate and frame design mainly because graphene is produced in chemical vapor deposition (CVD) reactors as sheets. Large CVD reactors can easily produce 10 cm × 50 cm sheets. To minimize concentration polarization and to reduce feed pressure drop, the feed channel gap should be optimized. In this study, we consider channel gap of 164 μm. The width of the membrane sheets is supposed to be kept as 50 cm, and the total area is calculated with the aid of the optimization model. The number of sheets in parallel is adjusted to maintain a certain flow velocity in the feed side (usually between 1 and 2 m/s [35]).

3.3. Vacuum pumps and compressors efficiency

The efficiency of the compressors in the layout with feed compression as well as of the blower in the layout with permeate vacuum is taken as 85% [10,11]. Concerning the latter layout, the permeate pressure is varied from 0.01 to 0.50 bar. Since achieving vacuum pressures lower than 0.1 bar at large scale is challenging, we referred to pumping solutions already in use in other industrial sectors where vacuum is implemented at a large scale such as in the food sector. In fact, in the food industry, vacuum down to 0.001 bar, is used for food transport, processing (e.g., vacuum cooling [36] or drying [37,38]) and packaging [39] and for cleaning operations. In addition, vacuum technology is widely applied for the evacuation of containers, vessels and lines in many industrial processes such as casting processes or semiconductor production [40]. To achieve this, it is crucial to select a proper combination of vacuum pumps, depending on the flow rates and the degree of vacuum required. We made a preliminary analysis to select the most suitable pumps, taking into account the large scale of operation (high pumping speed required) and the significant pressure ratio (high energy efficiency required). As a result, we selected two possible pumping solutions: dry screw pumps and the combination of roots pumps and LRVPs. In fact, LRVPs cannot be used for pressures lower than ca. 0.10 bar at a reasonable scale but can be coupled as backing pumps to roots blowers. On the one hand, the main advantage of the dry screw pumps is a higher energy efficiency, especially when optimized designs, as multi-stage gradational lead screw pumps, are used [41]. On the other hand, LRVPs are particularly suitable for high-scale processes and their investment cost is lower than that of screw pumps when a high pumping speed is needed [42]. Generally speaking, the LRVPs are preferable for large-scale processes as their large capacity leads to a lower number of pumps in parallel with respect to dry pumps with smaller capacities, thus to a lower total investment cost [42]. In addition, in the presence of a wet feed, the water vapor in the gaseous stream condensates in the LRVPs (typically working with liquid water at ambient temperature), whereas it may create issues in the screw pumps since the formation of liquid drops may impose mechanical forces that damage the pump and shorten its lifetime and may reduce the energy efficiency. Therefore, for all vacuum pump configurations, we employ and simulate the combination of roots blowers (in series) and LRVPs, where permeate runs first into roots pumps and then into LRVP. It is worth mentioning that the high capacity of the selected vacuum pumps allows for configurations with a limited number of pumping units (for the large-scale capture process, the number of LRVPs ranges between 20 and 30), which are feasible to implement. We fix the inlet pressure for LRVPs as equal to or greater than 0.10 bar. The number of roots-pump stages depends on the permeate pressure (ranging from 0.01 to 0.10 bar) and the compression (increase in pressure) that a single roots stage can realize. For large-scale roots pumps, the typical compression is 0.03 bar. Therefore, we adopt this value for the simulation.

The efficiency of the roots pumps has been taken equal to 60%, in agreement with the data given by the supplier for roots pumps with high pumping speed and ability to compress by 0.03 bar. We consider two different scenarios for the LRVPs: in the first scenario, we take an efficiency of 60%, in agreement with equation (20) [10]:

$$\eta_{vacuum} = 0.1058\ ln\left(\frac{P_{low}}{P_{high}}\right) + 0.8746 \tag{20}$$

This expression gives an efficiency of around 60% when P_{low} is equal to 0.10 bar and P_{high} is equal to 1 bar, which is the typical operating condition of the LRVPs in our systems. This value of efficiency is in line with the values reported for lower-scale LRVPs obtained by calculating the liquid losses with the method proposed by Huang et al. [32].

In the second scenario, we consider a lower and very conservative value of efficiency, equal to 40%. This efficiency has been estimated by taking the data of power consumption given by the supplier for the largest LRVPs (more detail in the supplementary materials, Figure S2). The efficiency can be improved by tuning the geometry of the impeller to reduce the power losses in the liquid ring, however, we also consider this low efficiency to understand the worst-case scenario. The main technical parameters used for the simulations are collected in Table 1.

3.4. Economic parameters

The main economic parameters used in equations (14)–(19) are reported in Table 2. For the estimation of the investment cost of the vacuum pumps (equation (17)), we consider two different reference points (pumping speed at the inlet pressure and cost) for the roots pumps and for the LRVPs, as listed in Table 2. These values are based on quotations provided by the leading pump suppliers (see supplementary materials, Figure S1). Also, the design pumping speeds corresponding to commercially available high-scale roots and LRVPs are reported in Table 2.

Finally, it is worth mentioning that we consider a much higher specific cost of the membrane (500 $/m^2) than those typically reported for polymeric membranes (ranging between 30 and 80 $/m^2). This cost includes membrane housing, piping and instrumentation and it has been

Table 1
Summary of the technical parameters used for the simulations.

Technical parameters	Value	Units
$X_{CO2,in}$	0.10	[−]
Q_{in}	4385	[mol/s]
T	50	[°C]
$X_{H2O,in}$ (wet feed)	0.15	[−]
CO_2 permeance	10000	GPU
CO_2/N_2 selectivity	30	[−]
CO_2/H_2O selectivity	1	[−]
CO_2/O_2 selectivity	12.6	[−]
η_{Roots}	60	[%]
η_{LRVP}	40–60	[%]
$\eta_{compressor}$	85	[%]

Table 2
Summary of the economic parameters used for the simulations.

Economic parameter	Value	Units
$C_{spec,m}$	500	[US$/m^2]
$C_{spec,\ power}$	0.05	[US$/kWh]
$C_{roots,ref}$	30,000	[US$]
$Q_{in,roots\ ref}$	4500	[m^3/h]
$Q_{in,design\text{-}roots}$	12,800	[m^3/h]
$C_{LRVP,ref}$	150,000	[US$]
$Q_{in,LRVP\ ref}$	5250	[m^3/h]
$Q_{in,design\text{-}LRVP}$	20,000	[m^3/h]
Operating hours	8000	[h/y]

estimated by taking into account the costs of manufacturing of the graphene membrane, and in particular the cost of the chemical vapor deposition setup, the chemicals including copper foil, the cost of the mechanically-reinforcing support layers, and the equipment required. Also, this estimation is particularly conservative to account for the current technology readiness level (4–5) to produce the NSLG membranes.

4. Results and discussion

Since a large-scale separation process based on the high-performance graphene membranes has never been reported, a number of configurations are considered in this work to select the optimal. Firstly, a preliminary comparison of double-stage configurations with either feed compression or permeate vacuum and either with or without recycle of the 2nd retentate is presented. Secondly, the specific CO_2 costs are minimized under two scenarios of LRVP efficiency. Next, the specific area, specific energy consumption, and CO_2 capture penalty required with dry and wet feeds are compared, and a sensitivity analysis is carried out by varying the inlet CO_2 concentration. Finally, the impact of non-ideal phenomena, as concentration polarization and pressure drops, on specific area, specific energy consumption, and CO_2 capture penalty is assessed for one case study.

4.1. Feed compression vs vacuum in permeate

To compare the configuration using feed compression with that using vacuum in permeate, two cases for each configuration corresponding to two pressure ratios (10 and 20) are considered. This translates into permeate pressure of either 0.05 or 0.10 bar, and feed pressure of 1 bar in both stages for the vacuum case (Fig. 5A). For the feed compression case, the feed pressure is either 20 or 10 bar in both stages, whereas the permeate pressure is set to 1 bar (Fig. 5B). Different specific membrane areas, energy consumption, and capture penalty are required to achieve a fixed recovery and purity of 80% (Fig. 5C, D, and E). Generally, the specific area (Fig. 5C) increases when the ratio between feed pressure and permeate pressure (pressure ratio) decreases because of the lower driving force. The specific area required with the vacuum is 7- to 10-fold higher than that required with the compression, because of the lower operating feed pressure. Conversely, the specific energy (Fig. 5D) required by the feed compression is 2- to 4-fold higher than that required to create the vacuum in permeate, even with the lower efficiency of vacuum pumps (60%) with respect to that of compressors (85%). These findings are in line with the literature [4,10]. However, while in the literature, the higher specific area for the vacuum configuration led to higher specific CO_2 cost with respect to the compression configuration, we find that the vacuum configuration has always lower CO_2 capture penalty (Fig. 5E). The reason is the higher CO_2 permeance of the NSLG membrane (10000 GPU) in comparison with those reported in the literature (from 200 to 500 GPU [4,10]). The higher permeance leads to a lower membrane area required for both vacuum and compression configurations. Therefore, the cost of membranes only accounts for 30–40% of the total cost in the vacuum scenario, whereas in the literature, this accounted for 60–75% of the total cost [10]. For this reason, despite the higher membrane area required with the vacuum configuration, a lower capture penalty is predicted. Therefore, we use vacuum configuration for further simulations. Furthermore, from the comparison of the performances of a double-stage system with and without recycle of the second retentate, it is possible to conclude that the configuration with recycle reduces the power requirement and capture penalty because it allows for achieving the target recovery and purity at higher permeate pressures (more details are reported in the supplementary materials, Section 3). Thus, in line with other works in the literature focused on polymeric membrane-based carbon capture, the double-stage with recycle configuration will be used for the following simulations.

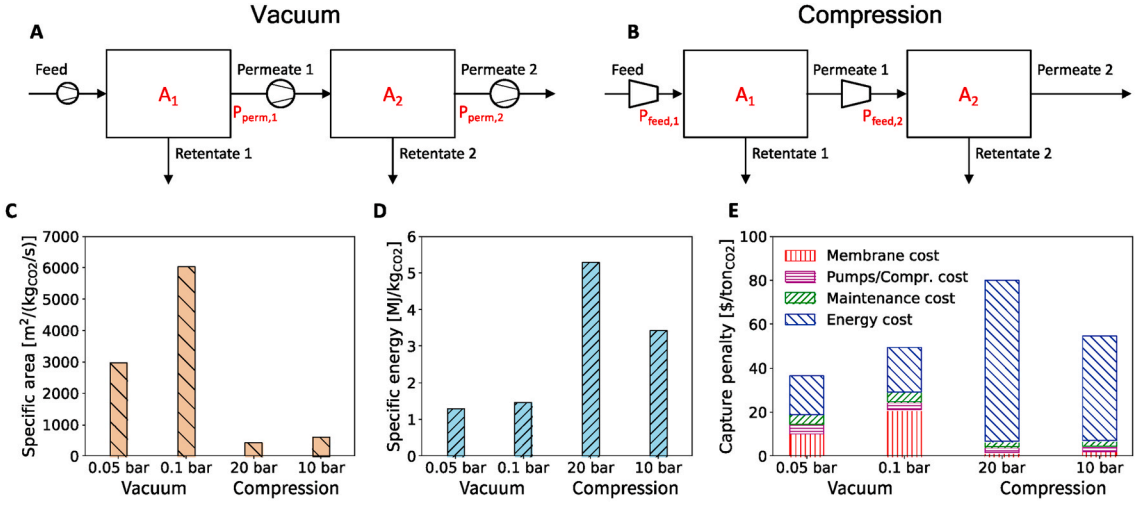

Fig. 5. Comparison between double-stage processes handling a dry feed with 10% CO_2. (A) With vacuum pumps for the permeate streams, and (B) with compressors for the feed streams. Bar charts with (C) specific area, and (D) specific energy consumption required to achieve recovery = 80% and purity = 80%, calculated for the vacuum configuration with a permeate pressure equal to 0.05 or 0.10 bar in both stages and for the compression configuration with a feed pressure equal to 20 or 10 bar in both stages. (E) Bar chart with the four main terms of cost per ton of CO_2 for the vacuum configuration with a permeate pressure equal to 0.05 or 0.10 bar in both stages and for the compression configuration with a feed pressure equal to 20 or 10 bar in both stages.

4.2. Capture penalty from the dry feed at variable pressures – Scenario 1

With optimized process configuration i.e., two-stage with recycle, a systemic study is carried out to minimize the capture penalty from a dry feed (10% CO_2) to achieve recovery and purity targets of 90%, assuming a vacuum pump efficiency of 60%.

Fig. 6A represents the region in the specific-energy/specific-area plane where the target for recovery and purity is met for the range of permeate pressure comprised between 0.01 and 0.10 bar. Interestingly, the needed specific area ranges from 2.5×10^3 to 6×10^3 $m^2/(kg_{CO2}/s)$, much lower than that reported in the literature, in the order of 10^5 $m^2/(kg_{CO2}/s)$, to achieve the same target, and using membranes yielding the same selectivity [14]. This is because the permeance used in the literature was taken from the Robeson's upper bound for CO_2/N_2 separation (110 GPU for CO_2/N_2 selectivity of 30) [43], whereas the permeance yielded by the NSLG membranes is orders of magnitude higher.

The lower bound of the attainable region contains all points corresponding to a permeate pressure in the second stage ($P_{perm,2}$) of 0.10 bar, i.e. the highest permeate pressure considered in Fig. 6A. A lower permeate pressure and a larger area are required in the first stage to achieve a high recovery. Conversely, the second stage can operate with a higher permeate pressure and yet requires a smaller membrane area because the CO_2 feed concentration to the second stage is high (ca. 50%). Since a lower vacuum (higher permeate pressure) leads to lower power consumption, the points at $P_{perm,2}$ equal to 0.10 bar correspond to the most feasible operating conditions, which will be adopted for further investigation. In addition, it is worth noting that, in the whole range of permeate pressure investigated (0.01–0.50 bar), the capture penalty is almost constant when $P_{perm,2}$ ranges from 0.10 to 0.15 bar, then it starts to increase significantly at higher $P_{perm,2}$, because of the rise of the required membrane area. Conversely, as we show later, when the electricity cost is higher, as in the case of cement and steel plants, permeate pressures in the second stage higher than 0.10 bar are more favorable.

Fig. 6B and C compare the terms of capture cost and power consumption of the systems along the lower bound in Fig. 6A with fixed $P_{perm,2} = 0.10$ bar and variable $P_{perm,1}$. Firstly, Fig. 6B shows that the membrane cost has the biggest increase with increasing $P_{perm,1}$ because the needed area increases with reducing the driving force. Secondly, the cost of pumps and blowers decreases with increasing $P_{perm,1}$ because the inlet volumetric flow rate lowers; thus, fewer pumps in parallel are required. Also, the number of stages for roots pumps reduces because the needed pressure growth up to LRVP suction pressure (0.10 bar) reduces. The maintenance cost has a very slight variation: it first decreases, driven by the decrease of the cost of pumps, and then increases driven by the increase of the membrane cost. Finally, the energy cost is always the largest term, and becomes comparable to the membrane cost at higher $P_{perm,1}$. The variation of the energy cost can be explained by looking at the trend of the total power requirement (dashed black line, Fig. 6C). The total power shows a minimum at $P_{perm,1} = 0.02$ bar and this trend, together with the increasing trend of the membrane cost with $P_{perm,1}$ leads to a minimum capture penalty of 41.5 $/ton$_{CO2}$ for $P_{perm,1} = 0.02$ bar. Such power corresponds to 21.5% of the total power produced by a power plant emitting around 0.5 million tons of CO_2 per year (125 MW of electricity produced).

Concerning the pumping units, the system with $P_{perm,2} = 0.10$ bar includes feed blowers, a certain number of stages of roots pumps in series (from 0 to 3 depending on $P_{perm,1}$) feeding to LRVPs for the first stage. For the second stage, LRVPs are used by themselves without the roots pumps. Fig. 6C shows that the power required by the blowers as well as that required by the 2nd and the 3rd stages of roots pumps (Roots 1.2 and 1.3, when they are present), does not vary significantly with $P_{perm,1}$. The power required by the LRVPs in the second stage (LRVP 2) is constant because the permeate flow rate is always the same once the recovery, purity, and $P_{perm,2}$ are fixed.

Therefore, the trend of the total power with increasing $P_{perm,1}$ is mostly due to the variation of the power required by the first stage of roots pumps (Roots 1.1) and by LRVPs in the first membrane stage (LRVP 1). Briefly, the power required by Roots 1.1 decreases with the increase of $P_{perm,1}$ because of the lower inlet volumetric flow rate. On the other hand, the power required by LRVP 1 (inlet pressure fixed at 0.10 bar) increases with the increase of $P_{perm,1}$. This is because the required membrane area grows with $P_{perm,1}$ and this leads to an increase of the molar flow rate of permeate. The opposite behavior in energy consumption of Roots 1.1 and LRVP 1 brings to a minimum of the total power at $P_{perm,1} = 0.02$ bar.

Fig. 7 reports the flow rates and concentrations of the retentate and the permeate streams generated within the optimal configuration, corresponding to the minimization of the capture penalty to 41.5 $/ton$_{CO2}$. This cost is competitive with the state-of-art absorption-based capture (48–111 $/ton$_{CO2}$) [7]. Moreover, despite the high specific membrane cost of NSLG considered in this study (500 $/m^2), the capture penalty falls within the range of capture cost reported using polymeric membranes [10,12]. The impact of the terms of costs relevant to each single stage on the global ones with this configuration is shown in the supplementary materials, Figure S4.

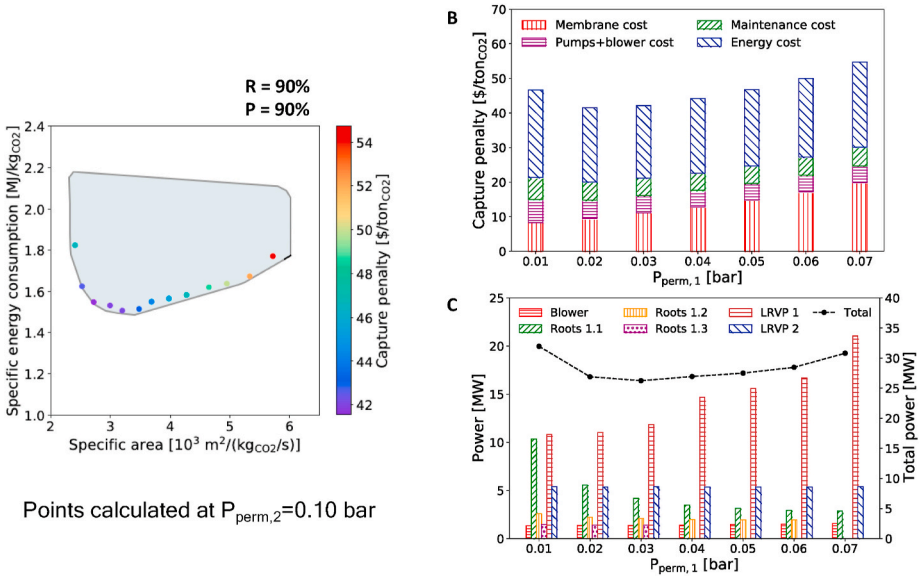

Fig. 6. Techno-economic analysis for CO_2 capture from dry feed (10% CO_2, inlet flue gas flow rate equal to 4385 mol/s). (A) Attainable region (recovery = 90%, purity = 90%) on the specific-energy-consumption/specific-area plot for the double-stage with recycle configuration. The colored points correspond to a permeate pressure in the second stage equal to 0.10 bar (the highest vacuum pressure investigated) and the colors are referred to the color bar of the total CO_2 capture penalty. (B) Bar chart with the terms of cost of the systems corresponding to the colored points (variable permeate pressure in the first stage, fixed permeate pressure in the second = 0.10 bar). (C) Bar chart with the power consumption of each pumping unit and the total power of the systems corresponding to the colored points (variable permeate pressure in the first stage, fixed permeate pressure (0.10 bar) in the second stage). (For interpretation of the references to color in this figure legend, the reader is referred to the Web version of this article.)

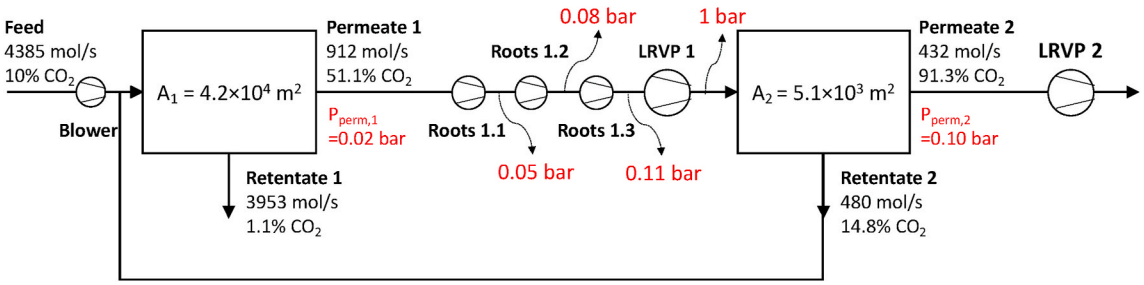

Fig. 7. The layout of the double-stage with recycle process with the membrane areas and permeate pressures corresponding to the lowest CO_2 capture cost. The system is designed to achieve a recovery of 90% and a purity of 90% while processing a dry feed (10% CO_2, 90% N_2).

4.3. Capture penalty from the dry feed at variable pressures – Scenario 2

When the efficiency of the LRVPs decreases from 60% (scenario 1) to 40% (scenario 2), the specific energy consumption for capture increases significantly, especially since the power consumption of the LRVPs is a significant fraction of the total. Fig. 8A shows the net increase of the specific energy consumption for scenario 2. As a consequence, the lowest CO_2 capture penalty increases to 48.1 $/ton$_{CO2}$.

In order to reduce the costs, we investigate an alternative option where the driving force in the second stage is generated by feed compression instead of vacuum in the permeate. In the first stage, vacuum is still the optimal solution because this stage operates with a significantly higher pressure ratio and feed compression in this stage would be much more expensive. To compare the area and the power requirements of this configuration, we simulate the process using a similar feed to the second stage as that obtained in Fig. 7 (Permeate 1 with a CO_2 concentration of 50%).

The use of a compressor instead of the vacuum in the second stage impacts the needed membrane area and energy consumption. As already shown in Fig. 5, the area required with the compressor is always lower than that required with the vacuum pumps. This is also evident in this case, as revealed by the comparison of the membrane area required for the same separation with vacuum (Fig. 8B) and with compression (Fig. 8C). However, it is important to note that the membrane area in the second stage is only a small fraction of that needed in the first stage, thus a reduction in the area of the second stage is not expected to have high impact on the capture penalty (as also evident from Supplementary Figure S4).

It was previously shown that vacuum pumps with an efficiency of 60% consume less energy than compressors (Fig. 5). However, since the efficiency of the LRVPs is lower (40%) in this scenario, there may be a range of feed pressure at which the power required by the compressor is lower than that required by LRVPs. In fact, as shown in Fig. 8D, there is a wide range of feed pressures (lower than 10 bar) in which the power consumption of the compressor is lower than that of the LRVPs operating with the same inlet conditions as the pumping unit of the second stage in Fig. 7 but with an efficiency of 40%. The layout showing the lowest capture penalty is the one with the lowest possible feed pressure in the second stage since a lower pressure corresponds to lower energy consumption. It should be noted that a lower feed pressure requires a higher membrane area. However, the area, and therefore, the cost of the membrane in the second stage is almost negligible since the area required in the second stage with compression is 5 times lower than that required with the vacuum.

Overall, it is possible to reduce the capture penalty in the scenario of low efficiency of LRVPs (40%) by switching to a combination of permeate vacuum in the first stage and feed compression in the second stage (Fig. 8E and F). The layout, with the areas required to achieve the recovery and purity targets when a pressure of 6 bar is used for the second stage, presents a capture penalty of 45 $/ton$_{CO2}$. A detailed comparison of the costs of the vacuum-vacuum and vacuum-compressor configurations is shown in the supplementary materials, Figure S5.

4.4. Simulation with wet feed

To account for the presence of water vapor in the flue gas, we perform simulations using a wet feed stream (10% CO_2, 15% water vapor, 3% O_2 and 72% N_2). CO_2-selective membranes, including functionalized NSLG membranes, are permeable to water vapor. On the basis of experiments performed in our laboratory and in line with other literature [1,11,52], we assume water vapor permeance equal to that of CO_2 and a CO_2/O_2 selectivity of 12.6. This implies that a significant amount of water vapor is present in the permeate stream, which increases the pumping load. In addition, the permeate flow rate is slightly increased by the presence of O_2, since the membranes are more permeable to O_2 than N_2. However, the presence of other components in the permeate also benefits the process to some extent because the CO_2 concentration on the permeate side becomes smaller, mostly from dilution in water vapor. This leads to a higher driving force for CO_2 permeation across the membrane and, eventually, to a higher CO_2 flux.

Fig. 9A and B compare permeate flux and permeate concentration of CO_2 from the dry and the wet feeds, and of water vapor from the wet feed. The flux of CO_2 with wet feed is higher than that with dry feed for the first one-third of the membrane length attributing to the dilution from water vapor. The higher flux leads to a steeper decrease of the feed concentration (as shown in the Supplementary Figure S6), thus the rest of the membrane length presents a slightly lower or comparable flux with respect to the case with the dry feed. The water vapor flux is always higher than that of CO_2 since (i) its permeance is equal to that of CO_2, and (ii) it has a higher concentration in the feed.

CO_2 concentration in the permeate shows a stronger reduction along the membrane length for the dry feed compared to the wet feed because the initial (across the first length element) permeate concentration with the dry feed is much higher, whereas flux in the last element is close to zero in both cases. The higher flux found with the wet feed should lead to a higher recovery when the membrane area is the same. To explore this further, we simulate the process with wet feed using the same configuration (membrane area and permeate pressures) as that for the dry feed as reported in Fig. 7. We indeed find that the recovery in the first stage as well as the total recovery is higher when the wet feed is used (Fig. 9C and D). Therefore, it provides an opportunity to reduce the membrane area and consequently the membrane investment costs, while meeting the recovery target. However, as mentioned before, the presence of a significant amount of water in the permeate would increase the energy consumption of vacuum pumps, especially when a low permeate pressure is used. Therefore, we further optimize the membrane area and the permeate pressures to minimize the capture cost. The detailed results of the cost minimization are reported in the supplementary materials (Figure S7). The resulting membrane area, permeate pressures, flow rates, and concentrations are shown in Fig. 9E.

It is worth mentioning that the optimized value of $P_{perm,1}$ (0.05 bar) for wet feed is higher than that used with the dry feed (0.02 bar). This shift to a higher permeate pressure in wet feed is driven by a reduction in the energy consumption of the vacuum pumps which have an added load of water vapor. For this reason, the required membrane area is slightly

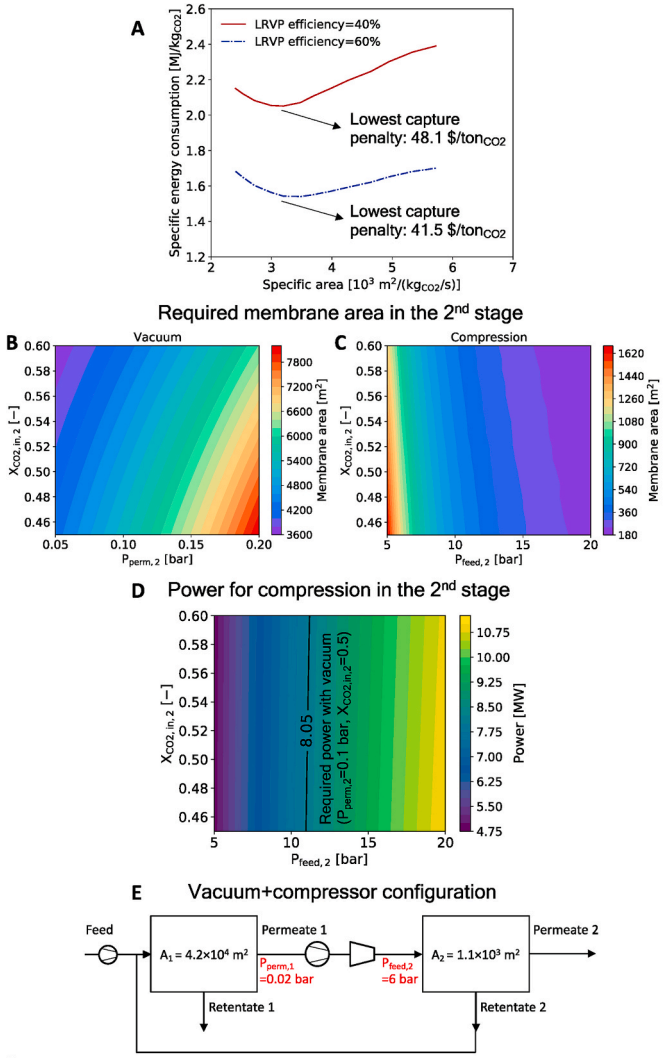

F

	Vacuum (1st) + vacuum (2nd)	Vacuum (1st) + compression (2nd)
Specific energy consumption	2 MJ/kg$_{CO2}$	1.9 MJ/kg$_{CO2}$
CO_2 capture penalty	48 $/ton$_{CO2}$	45 $/ton$_{CO2}$

Fig. 8. Techno-economic analysis for scenario 2 when the LRVP efficiency is 40% (10% CO_2, inlet flue gas flow rate equal to 4385 mol/s). (A) Trends of specific energy vs. specific area with $P_{perm,2}$ = 0.10 bar with LRVP efficiencies of 60% and 40%. Comparison of the required membrane area for the second stage via heat maps referred to systems where vacuum is used (B) and where compression is used (C) for the second stage. (D) Heat map of the power required for the compression of the feed entering the second stage at variable inlet CO_2 concentration and feed pressure to ensure the recovery and purity targets. Black line: power required with the vacuum (η_{LRVP} = 40%) at the operating conditions in (A) for the lowest capture penalty. (E) Optimized double-stage with recycle configuration with vacuum in the first stage and compression in the second stage, indicating operating conditions and the needed membrane areas to achieve 90% recovery and 90% purity (F) Table with the comparison of the specific energy consumption and the CO_2 capture penalty when one uses only vacuum pumps ($P_{perm,1}$ = 0.02 bar, and $P_{perm,2}$ = 0.10 bar) and when one uses the optimized configuration shown in (E).

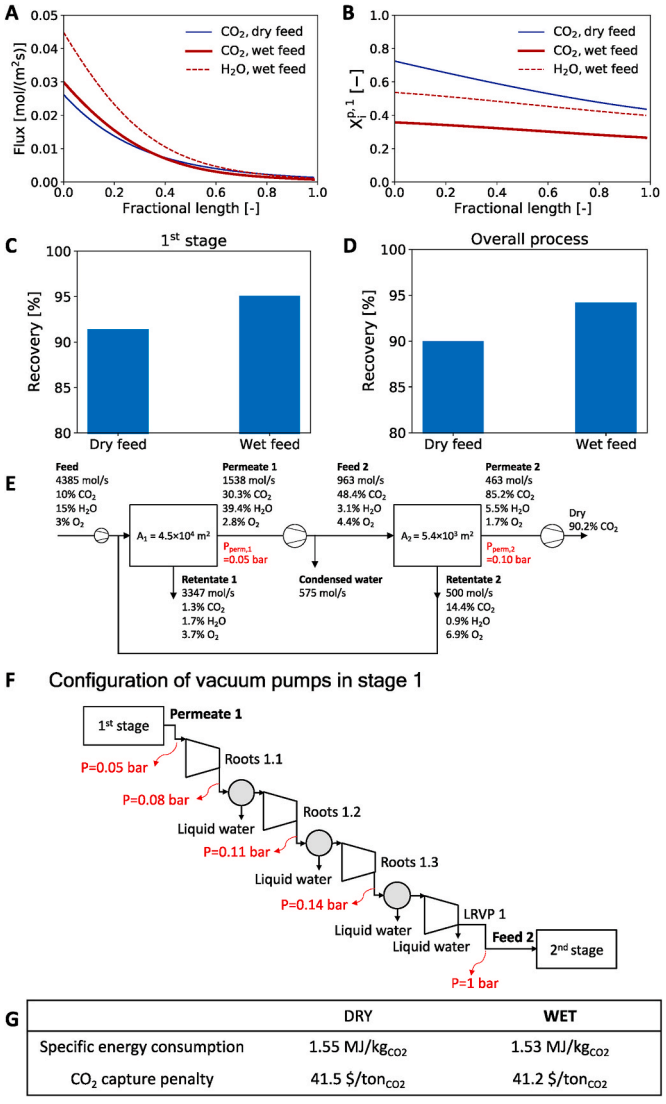

G

	DRY	WET
Specific energy consumption	1.55 MJ/kg$_{CO2}$	1.53 MJ/kg$_{CO2}$
CO_2 capture penalty	41.5 $/ton$_{CO2}$	41.2 $/ton$_{CO2}$

Fig. 9. (A) Comparison of the CO_2 flux from the dry feed (10% CO_2, 90% N_2) and of CO_2 and H_2O fluxes from the saturated wet feed at 50 °C (10% CO_2, 15% H_2O, 3% O_2, 72% N_2) along the fractional length of the membrane in the first stage. (B) Comparison of the bulk permeate concentration of CO_2 with the dry feed and of CO_2 and H_2O with the saturated wet feed along the fractional length of the membrane in the first stage. Bar charts comparing the recovery obtained from dry and wet feeds from the first stage (C) and from the overall process (D) using optimized membrane areas and permeate pressures that minimized the capture cost for the dry feed (Fig. 7). (E) The layout of the optimized (minimizing CO_2 capture penalty) process for the wet feed listing permeate and retentate compositions, flow rates, membrane areas, and permeate pressures. (F) Configuration of the vacuum pumps for the first stage including the condensers to remove water vapor. (G) Table with the comparison of specific energy consumption and CO_2 capture penalty with dry feed (using the same configuration as in Fig. 7) and with wet feed (using configuration shown in (E)).

higher than that required with the dry feed (see Fig. 7) but it is still lower than the area that would be required with the dry feed if $P_{perm,1}$ was set to 0.05 bar.

Furthermore, in this layout, most of the water vapor present in the 'Permeate 1' stream can be removed before the second membrane stage. This can be realized by using multistage roots pumps, where intermittent coolers are added to gradually reduce the water concentration, and thus to reduce the flow rate entering in the subsequent stages of the pumps. Similar systems consisting of multi-stage vacuum pumps and interstage coolers are often used for various industrial applications to reduce the risk of condensation inside the dry pumps and to increase their suction capacity [44,45]. This gradual reduction in the flow rate of water vapor is beneficial because it decreases the net inlet molar flow rate for the subsequent stage of the pump, and, consequently, the capital cost of the pump. Fig. 9F shows the proposed configuration of the vacuum pumps in the first membrane stage, comprised of three stages of roots pumps and one stage of LRVP. Between each stage of

roots pumps, a cooler is located to condense a part of the water vapor, reducing the concentration of water vapor entering LRVP. In fact, LRVP has the highest energy consumption and the reduction of its inlet flow rate has a strong impact on the required power and the capture penalty. Since most of the water vapor entering the LRVP condenses in the pump itself, which operates with liquid water at 25 °C, the flow rate and CO_2 concentration of the stream leaving the LRVP and fed to the second membrane stage are very similar to those optimized for the dry feed (Fig. 7).

The total power and the capture penalty for the wet feed are reported in Fig. 9G. Overall, the power consumption and the capture penalty come out to be very close to those with the dry feed.

4.5. Sensitivity analysis to inlet CO_2 concentration

The inlet CO_2 molar fraction used for the simulations so far is 10%. The literature typically uses higher concentration, e.g., 11.6% [12] and 13.5% [1,4,11] for the techno-economic analysis of the membrane process. Therefore, we perform a sensitivity analysis to assess the variation of the capture penalty with the inlet CO_2 concentration while keeping the total amount of CO_2 captured constant at 0.5 million ton per annum. The permeate pressures are kept fixed, the same as those reported in Fig. 9, i.e., 0.05 and 0.10 bar. The resulting capture costs from the sensitivity analysis, highlighting the contribution from membranes and pumps investment costs, energy cost, and maintenance cost, are reported in Fig. 10.

The higher CO_2 concentration in the feed leads to a higher driving force across the membrane. Thus, smaller membrane areas can achieve the same separation, leading to a lower membrane cost. In addition, the higher inlet CO_2 concentration corresponds to lower feed flow rates for the same total CO_2 productivity (amount captured), thus the number of pumps in parallel and the power requirement reduce significantly. Therefore, capital costs as well as energy costs decrease. Overall, the capture penalty significantly decreases with increasing the CO_2 feed concentration. For a wet feed with an inlet CO_2 concentration of 13.5%, the capture penalty reduces to 31.8 $/ton$_{CO2}$. This cost is competitive with the state-of-the-art-absorption process [5,7] and with polymeric membranes-based separation processes proposed in the literature [1, 11]. This further demonstrates how the capture process based on NSLG membranes is a valid option for the postcombustion carbon capture.

Finally, the flue gas produced in cement and steel plants has even higher CO_2 fractions, which range from 20 to 30% [46]. Baker et al. proposed a double-stage membrane process to recover 80% of the produced CO_2 (800 ton/day) from flue gas with an inlet CO_2 concentration of 25%. For this case, they reported a capture penalty of 43.2 $/ton$_{CO2}$, a specific area of 12.2 × 10^3 m^2/(kg$_{CO2}$/s) and a specific energy consumption of around 1 MJ/kg$_{CO2}$ [46]. Considering an analogous system with the CO_2 permeance and CO_2/N_2 selectivity of NSLG membranes (10000 GPU and 30, respectively), we find a specific area of 3.1 × 10^3 m^2/(kg$_{CO2}$/s) and a specific energy consumption of around 0.66 MJ/kg$_{CO2}$. The lower specific area and energy consumption, due to the higher CO_2 permeance and selectivity (Baker et al. had CO_2 permeance of 1500 GPU and CO_2/N_2 selectivity of 25), lead to a lower capture penalty of 23.5 $/ton$_{CO2}$. This comparison allows the first assessment of the feasibility of using NSLG membrane for CO_2 capture from cement and steel plants flue gas. However, this value of capture penalty has been estimated, in analogy with the literature, at an electricity cost of 0.05 $/kWh.

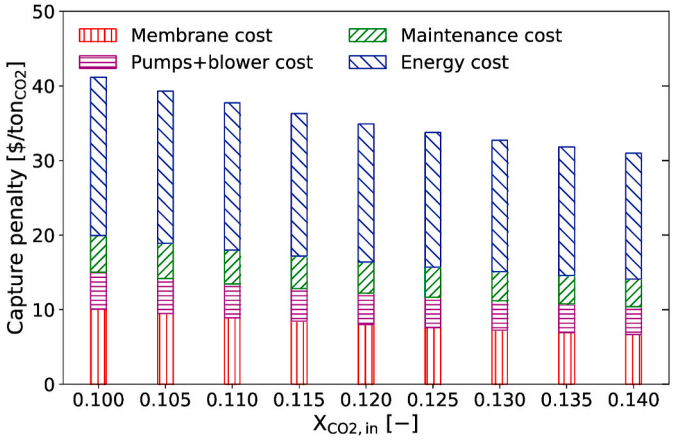

Fig. 10. Bar chart showing capture penalty at various inlet CO_2 concentrations (the concentration of H_2O and O_2 in the feed are fixed at 15% and 3% respectively, the remainder is N_2). The total amount of CO_2 produced is fixed at 0.5 million ton/y and the inlet molar flow rate of the feed changes depending on the CO_2 concentration. The permeate pressures are fixed as 0.05 and 0.10 bar in the first and the second stage, respectively.

Since additional costs should be considered for electricity consumers different than the power plant itself, we investigate the impact of the electricity cost on the optimal double-stage configuration and on the capture penalty to achieve the recovery and purity targets of 90%. We consider a wide range of electricity costs, from 0.01 to 0.20 $/kWh, and fix the pressure in the permeate channel of the first membrane stage to 0.06 bar, which minimizes the capture penalty at any $P_{perm,2}$. For each value of electricity cost, we then optimize the system configuration ($P_{perm,2}$ and membrane areas) to minimize the capture penalty.

As shown in Fig. 11A, the rise of $P_{perm,2}$ corresponds to a decrease of the energy requirement in almost the entire range of pressure but also to an increase in the membrane area. The increase of the energy requirement at the highest values of permeate pressures is due to the larger flow rates to be compressed in the presence of high membrane areas. Therefore, at higher electricity costs (Fig. 11B), the optimal $P_{perm,2}$ increases and gets closer or equal to the one that minimizes the energy requirement, despite the larger membrane areas required.

Typical values of electricity costs for non-households consumers range from 0.10 to 0.20 $/kWh [47] and the corresponding minimum capture penalties range from 28 to 46 $/ton$_{CO2}$. Since it has been reported that a capture penalty of around 40 $/ton$_{CO2}$ has a limited impact on the cement and steel costs [46], the capture penalties in Fig. 11 further demonstrate the feasibility of employing NSLG membranes for these industries.

4.6. Impact of non-ideal phenomena

So far, the effect of non-ideal phenomena such as concentration polarization and pressure drops has been neglected because of the high diffusivity of the gaseous species, in line with most of the modelling studies about gas separation membrane processes in the literature [48]. However, in the presence of highly permeable membranes, these phenomena can be more significant and their effect needs to be quantified.

Concentration polarization reduces the driving force across the membranes because the concentration of the most permeable species at the feed-membrane interface results lower than that in the bulk for the presence of a boundary layer [49]. The concentration at the interface can be estimated from the mass transfer coefficient in the feed channel, related to the Sherwood number [50].

Pressure drop along the feed channel can lead to a decrease in the driving force because of the reduction in the feed pressure. The drop in feed pressure depends on the feed stream velocity and the friction factor [35]. The correlations used in this work to quantify concentration polarization and pressure drops are reported in the supplementary materials (Section 7).

To assess the impact of non-ideal phenomena on NSLG membrane-based capture process, we refer to a binary mixture with CO_2 concentration of 13.5% (commonly reported in the literature) and feed flow rate of 3247.5 mol/s, corresponding to 0.5 million ton/y of captured CO_2 with recovery of 90% and purity of 90%. The simulated system is a double-stage with recycle of the second retentate. Although the system

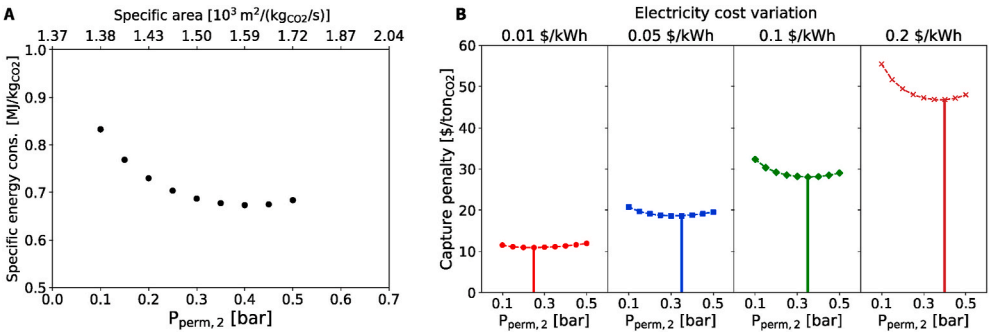

Fig. 11. (A) Specific energy consumption as a function of $P_{perm,2}$, and the corresponding specific area needed to achieve purity and recovery targets using the double-stage configuration with recycle. Inlet feed: 25% CO_2, 75% N_2. $P_{perm,1} = 0.06$ bar. Outlet CO_2 production: 0.5 million ton/y (corresponding to an inlet total molar flow rate of 1754 mol/s). (B) Capture penalty vs. $P_{perm,2}$ with different electricity cost values for the same system as in (A). The vertical bar highlights the $P_{perm,2}$ corresponding to the minimum capture penalty.

includes a blower to increase the feed pressure to 1.1 bar, conservatively, the feed pressure used for the simulations is kept equal to 1 bar, while the permeate pressures are equal to 0.02 and 0.10 bar, as in Fig. 7. The feed velocity in each membrane module is equal to 2 m/s, which corresponds to a laminar flow and allows to have pressure drops lower than the target of 1.5 psi/m given by the US Department of Energy [51].

Fig. 12 shows the trend of CO_2 flux in the first and in the second stage with the ideal case and when the losses due to non-ideal phenomena are included. Generally speaking, the impact of concentration polarization on the flux is stronger than that of pressure drops, which are limited also because of the small area required with NSLG membranes. Considering both concentration polarization and pressure drops, the average flux decreases by 11% in the first stage with respect to the ideal case. In the second stage, since the flux for the ideal case in the first discretization element is 12% higher, the driving force decreases more rapidly and an inversion of the trends occurs in the second part of the membrane sheet. The concentration profiles are shown in the supplementary materials, in Figure S10.

In terms of global outputs, the specific area, energy consumption and capture penalty for the ideal case are 1.9×10^3 $m^2/(kg_{CO2}/s)$, 1.27 MJ/kg_{CO2} and 32.7 \$/ton_{CO2}, respectively. Conversely, for the case with concentration polarization and pressure drops, these are 2.2×10^3 $m^2/(kg_{CO2}/s)$, 1.36 MJ/kg_{CO2} and 35.5 \$/ton_{CO2}. Therefore, the increase of capture penalty when non-ideal phenomena are included in the modelling is limited (lower than 10%) and the capture system is still in the feasibility region. In addition, in the future, the design of the membrane module will be optimized to further reduce any loss due to non-ideal phenomena.

4.7. Overview of the results and comparison with the literature

The values of minimum capture penalty found for the different cases are summarized in Table 3 together with the corresponding operating pressures. Overall, despite the high investment costs and the relatively low efficiency of the vacuum pumps, the separation process turns out to be feasible even when the inlet concentration of CO_2 is equal to 10%.

The optimal permeate pressure results from a number of tradeoffs between energy requirement and investment for membrane area and between different terms of power consumption [18]. It is worth noting that, when the permeate flow rates increase (as in the presence of wet feed) or when the electricity cost is higher (as for the cement and steel plant), the optimum pressure ratios diminish driven by the reduction of the operating cost due to energy requirement.

This work demonstrates that a membrane process with permeate under vacuum is more competitive than that with feed compression when the membranes have very high permeance. This marks a difference with respect to a number of other works dealing with less permeable membranes where feed compression resulted a more feasible strategy because of the high membrane area required with vacuum [4,10,11].

Table 4 compares the specific area, specific energy consumption, and capture penalty presented in this work with the literature. The results are relevant to the capture of CO_2 from wet feed, saturated with water vapor at 50 °C, and with concentration of CO_2 of 13.5% (except for [12], where the inlet CO_2 concentration is 11.8%). In analogy with the literature in Table 4, our results are estimated for target recovery and purity equal to 90 and 95%, respectively.

Concerning the cost composition, in this work, the membrane investment and the energy costs cover around 21 and 55% of the total cost, respectively. These correspond to a specific area of 2.06×10^3 $m^2/(kg_{CO2}/s)$ and an energy consumption of 1.37 MJ/kg_{CO2}. The specific area is lower than most of the values reported in the literature even when feed compression is considered [11] and is slightly higher than that obtained with high feed pressure (6 bar in the first stage and 30 bar in the second stage) and high CO_2 permeance (2600 GPU) [29]. The energy consumption is comparable with the values reported in the literature. With this regard, we note that (i) we used conservative values of efficiencies for vacuum pump and compressors compared to those reported in the literature [12,19,29], and (ii), in some cases, expanders are used to reduce the energy consumption of the compressors [29]. Lower energy consumption values are reported by Ramasubramanian et al. but they work with a limited pressure difference (1 bar in the feed

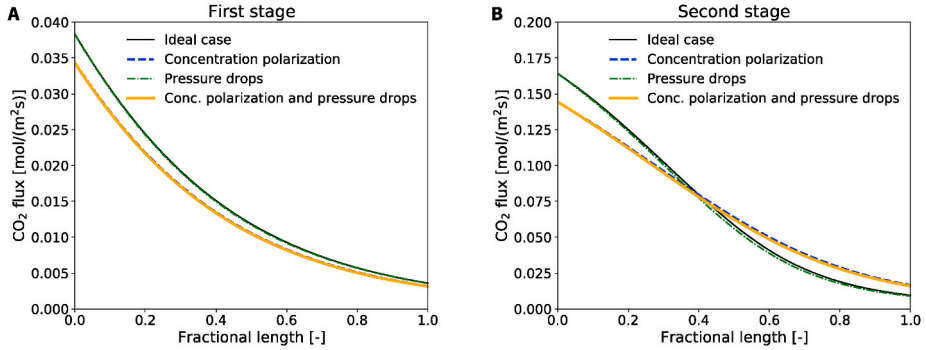

Fig. 12. Trends of CO_2 flux along the fractional length of (A) the first stage and (B) the second stage when considering the concentration polarization and pressure drop.

Table 3
Optimal operating pressures for each case study, with the corresponding capture penalty and investigated range of variables.

Case study	$P_{feed,1}$ [bar]	$P_{perm,1}$ [bar]	$P_{feed,2}$ [bar]	$P_{perm,2}$ [bar]	Capture penalty [$/ton$_{CO2}$]	Range of variables
Dry feed – Scenario 1	1	0.02	1	0.1	41.5	$P_{feed,1} = P_{feed,2}$:1 bar $P_{perm,1}$, $P_{perm,2}$:[0.01–0.5] bar
Dry feed – Scenario 2	1	0.02	6	1	45.0	$P_{feed,1}$:1 bar, $P_{perm,1}$:[0.01–0.5] bar $P_{feed,2}$: [5-20] bar, $P_{perm,1}$: 1 bar
Wet feed	1	0.05	1	0.1	41.2	$P_{feed,1} = P_{feed,2}$:1 bar $P_{perm,1}$, $P_{perm,2}$:[0.01–0.5] bar
Wet feed - $X_{CO2,in} = 13.5\%$	1	0.05	1	0.1	31.8	$P_{feed,1} = P_{feed,2}$:1 bar $P_{perm,1}$, $P_{perm,2}$:[0.01–0.5] bar
Cement, steel plant flue gas	1	0.06	1	0.35	28.0	$P_{feed,1} = P_{feed,2}$:1 bar $P_{perm,1}$, $P_{perm,2}$:[0.01–0.5] bar

Table 4
Comparison of the values of specific area, specific energy, and capture penalty obtained in this work with those reported in the literature. Our results are relevant to the case study of the wet feed with a CO_2 concentration of 13.5%, recovery of 90% and purity of 95%. The same concentration is used in all other works cited, except for [12] where a CO_2 concentration of 11.8% is used. The same recovery and purity are used in the other works.

	This work	[12]	[4]	[1]	[29]	[11]	[19]
CO_2 permeance [GPU]	10000	1000	1100	3000	2600	2916–519	4000
CO_2/N_2 selectivity	30	50	50	140	53.2	55–100	50
Membrane cost [$/m^2]	500	50	50	27	50	50	50
Electricity cost [$/kWh]	0.050	0.040	0.034	0.050	0.068	0.040	0.040
Specific area [10^3 m^2/(kg$_{CO2}$/s)]	2.06	14.50	33.80	14.0	1.12	5.90	6.37
Specific energy [MJ/kg$_{CO2}$]	1.37	1.10	0.92	0.70	0.92	1.70	1.12
Capture penalty [$/ton$_{CO2}$]	34.4	23.0	31.0	24.0	28.6	26.1	29.2

channel and 0.2 bar in the permeate) and membranes with high selectivity of 140 [1]. Concerning the capture penalty, the value obtained in this work with a CO_2 concentration in the feed equal to 13.5% is comparable or slightly higher to the values reported in the literature (the minimum value reported is 23 $/ton$_{CO2}$ for counter-flow modules [12]). However, the value of electricity cost used in this work (0.05 $/kWh) is higher than those used in other works (0.0337–0.04 $/kWh [4,11,12,19]). When we assume the electricity cost of 0.04 $/kWh, the capture penalty decreases from 34.4 to 30.6 $/ton$_{CO2}$. This is in line with the sensitivity analysis presented by Giordano et al., who showed that the change in the fuel cost (and consequently in the electricity cost) has the main impact on the capture cost [29]. Overall, the NSLG membrane-based separation process proposed is competitive with the optimal systems proposed in the literature.

5. Conclusions

We presented a techno-economic analysis for understanding the suitability of high-performance NSLG membranes for postcombustion carbon capture with a wide range of CO_2 concentrations in the feed, varying from 10 to 25%. The high CO_2 permeance from NSLG favored the use of vacuum pumps for permeate, reducing energy consumption compared to the scenarios using feed compression. The use of multistage roots pumps allowed to gradually reduce the flow rate to the subsequent pump by condensing the water vapor. Overall, despite a high assumed cost of these membranes ($500/m^2) and a conservative assumption of vacuum-pump efficiency, we show that the capture cost from the NSLG membranes is competitive to that from the commercial absorption process as well as those from the state-of-the-art polymeric membrane-based capture processes. These findings demonstrate that highly permeable NSLG membranes are an attractive alternative for post-combustion capture, especially where a decentralized operation is preferred, e.g., community-scale boilers. Further technological improvements in NSLG membranes are expected in the near future, which will drive down the energy consumption as well as the capture penalty; e.g., CO_2 permeance can be further improved by increasing the pore density and CO_2/N_2 selectivity can be further increased by narrowing down the pore-size-distribution.

Author statement

Micari, M.: Conceptualization, Methodology, Software, Writing – Original Draft; **Dakhchoune, M.**: Conceptualization, Writing – Review and Editing; **Agrawal, K.V.**: Conceptualization, Methodology, Supervision, Writing – Review and Editing.

Declaration of competing interest

The authors declare that they have no known competing financial interests or personal relationships that could have appeared to influence the work reported in this paper.

Acknowledgement

The authors would like to acknowledge the Valais Administration and host institute EPFL for supporting the project on carbon capture (Valais District Demonstrator Project). Parts of this work was supported by the Swiss Competence Center for Energy Research: Efficiency of Industrial Processes (SCCER-EIP). Authors are thankful to GAZNAT for providing data on flue gas composition from the CH4-fuelled boilers.

Nomenclature

$A_{membr,tot}$ total required membrane area [m^2]
C_{blower} cost of the blower [US$]
C_{compr} cost of the compressor [US$]
$C_{LRVP,ref}$ cost of the reference LRVP [US$]

C_{maint} cost for maintenance [US$/y]
C_{membr} cost of membrane sheets [US$]
C_{power} cost of the power required for the separation [US$/y]
C_{vacuum} cost of the vacuum pumps [US$]
$C_{roots,ref}$ cost of the reference roots pump [US$]
$C_{spec,m}$ specific cost of the membrane [US$/$m^2$]
$C_{spec,\ power}$ specific cost of electricity [US$/kWh]
$C_{vacuum,ref}$ cost of the reference generic vacuum pump [US$]
dA area of the membrane discretization element [m^2]
J_i flux of component *i* through the membrane [mol/(m^2 s)]
J_{tot} total flux through the membrane [mol/(m^2 s)]
K_c cost parameter for compressors [1/(m^3(STP)/s)]
P_{CO2} purity of CO_2 [-]
P_{compr} power consumption of the compressor [W]
P^f_i partial pressure of component *i* in the feed [Pa]
P_{feed} feed pressure [Pa] or [bar] if specified
P_{high} outlet pressure of compressor or vacuum pumps [bar]
P_{LRVP} power consumption of the LRVP [W]
P_{low} inlet pressure of compressor or vacuum pumps [bar]
P'^{P}_i partial pressure of component *i* in the permeate flux leaving the membrane [Pa]
P_{perm} permeate pressure [Pa] or [bar] if specified
P_{roots} power consumption of the roots pumps [W]
P_{tot} total power required [W]
$\mathbf{P}_i$ permeance of the component *i* [mol/(m^2sPa)]
Q_f molar flow rate of the feed stream [mol/s]
Q_f* molar flow rate of the stream fed to the 1st stage with recycle [mol/s]
$Q_{in,compr}$ flow rate entering the compressor [mol/s]
$Q_{in,design\text{-}LRVP}$ design pumping speed of the LRVP [m^3/h]
$Q_{in,design\text{-}roots}$ design pumping speed of the roots pump [m^3/h]
$Q_{in,LRVP}$ flow rate entering the LRVP [mol/s]
$Q_{in,LRVP\ ref}$ pumping speed of the reference LRVP [m^3/h]
$Q_{in,roots\ ref}$ pumping speed of the reference roots pump [m^3/h]
$Q_{in,vacuum}$ pumping speed of the vacuum pump [m^3/h]
$Q_{in,vacuumref}$ pumping speed of the reference generic vacuum pump [m^3/h]
$Q_{p,out}$ outlet molar flow rate of the permeate stream [mol/s]
Q_r molar flow rate of the retentate stream [mol/s]
$Q_{r,out}$ outlet molar flow rate of the retentate stream [mol/s]
$Q^{vol}_{in,\ roots}$ volumetric flow rate entering the roots pumps [m^3/s]
R gas constant [J/(mol K)]
R_{CO2} recovery of CO_2 [-]
T temperature [K]
$x_{CO2,in}$ molar fraction of CO_2 in the feed stream [−]
x^f_i molar fraction of component i in the feed stream [−]
x^{f*}_i molar fraction of component i in the feed of the 1st element with recycle [−]
x^p_i molar fraction of component i in the outlet permeate stream [−]
x'^{p}_i molar fraction of component i in the permeate flux leaving the membrane [−]
x^r_i molar fraction of component i in the retentate stream [−]
$x^{r,out}_i$ molar fraction of component i in the outlet retentate stream [−]
z axis corresponding to the membrane length

Greek letters

γ adiabatic index [−]
η_{compr} efficiency of the compressor [−]
η_{LRVP} efficiency of the LRVP [−]
η_{roots} efficiency of the roots pumps [−]

Acronyms

LRVP Liquid ring vacuum pumps
MEA CO_2 absorption technology with monoethanolamine
STP Standard temperature and pressure

Appendix A. Supplementary data

Supplementary data to this article can be found online at https://doi.org/10.1016/j.memsci.2021.119103.

References

[1] K. Ramasubramanian, H. Verweij, W.S. Winston Ho, Membrane processes for carbon capture from coal-fired power plant flue gas: a modeling and cost study, J. Membr. Sci. 421–422 (2012) 299–310, https://doi.org/10.1016/j.memsci.2012.07.029.

[2] J. Nørskov, A. Latimer, C. Dickens, Research Needs towards Sustainable Production of Fuels and Chemicals, 2019, https://doi.org/10.4324/9780429047237-18.

[3] E. Favre, Carbon dioxide recovery from post-combustion processes: can gas permeation membranes compete with absorption? J. Membr. Sci. 294 (2007) 50–59, https://doi.org/10.1016/j.memsci.2007.02.007.

[4] L. Zhao, E. Riensche, L. Blum, D. Stolten, Multi-stage gas separation membrane processes used in post-combustion capture: energetic and economic analyses, J. Membr. Sci. 359 (2010) 160–172, https://doi.org/10.1016/j.memsci.2010.02.003.

[5] G. Rochelle, Amine scrubbing for CO2 capture, Science 325 (2009) 1652–1654, https://doi.org/10.1126/science.1176731.

[6] A. Townsend, A. Gillespie, 2020 Thought Leadership - Scaling up the CCS Market to Deliver Net-Zero Emissions, Global CCS Institute, 2020.

[7] E.S. Rubin, J.E. Davison, H.J. Herzog, The cost of CO2 capture and storage, Int. J. Greenh. Gas Control. 40 (2015) 378–400, https://doi.org/10.1016/j.ijggc.2015.05.018.

[8] L. Peters, A. Hussain, M. Follmann, T. Melin, M.B. Hägg, CO 2 removal from natural gas by employing amine absorption and membrane technology-A technical and economical analysis, Chem. Eng. J. 172 (2011) 952–960, https://doi.org/10.1016/j.cej.2011.07.007.

[9] S. Roussanaly, R. Anantharaman, K. Lindqvist, H. Zhai, E. Rubin, Membrane properties required for post-combustion CO2 capture at coal-fired power plants, J. Membr. Sci. 511 (2016) 250–264, https://doi.org/10.1016/j.memsci.2016.03.035.

[10] D. Yang, Z. Wang, J. Wang, S. Wang, Potential of two-stage membrane system with recycle stream for CO 2 capture from postcombustion gas, Energy Fuels 23 (2009) 4755–4762, https://doi.org/10.1021/ef801109p.

[11] J. Xu, Z. Wang, Z. Qiao, H. Wu, S. Dong, S. Zhao, J. Wang, Post-combustion CO2 capture with membrane process: practical membrane performance and appropriate pressure, J. Membr. Sci. 581 (2019) 195–213, https://doi.org/10.1016/j.memsci.2019.03.052.

[12] T.C. Merkel, H. Lin, X. Wei, R. Baker, Power plant post-combustion carbon dioxide capture: an opportunity for membranes, J. Membr. Sci. 359 (2010) 126–139, https://doi.org/10.1016/j.memsci.2009.10.041.

[13] C.Y. Pan, Gas separation by permeators with high-flux asymmetric membranes, AIChE J. 29 (1983) 545–552, https://doi.org/10.1002/aic.690290405.

[14] P. Gabrielli, M. Gazzani, M. Mazzotti, On the optimal design of membrane-based gas separation processes, J. Membr. Sci. 526 (2017) 118–130, https://doi.org/10.1016/j.memsci.2016.11.022.

[15] R. Qi, M.A. Henson, Membrane system design for multicomponent gas mixtures via mixed-integer nonlinear programming, Comput. Chem. Eng. 24 (2000) 2719–2737, https://doi.org/10.1016/S0098-1354(00)00625-6.

[16] Á.A. Ramírez-Santos, M. Bozorg, B. Addis, V. Piccialli, C. Castel, E. Favre, Optimization of multistage membrane gas separation processes. Example of application to CO2 capture from blast furnace gas, J. Membr. Sci. 566 (2018) 346–366, https://doi.org/10.1016/j.memsci.2018.08.024.

[17] A.M. Arias, M.C. Mussati, P.L. Mores, N.J. Scenna, J.A. Caballero, S.F. Mussati, Optimization of multi-stage membrane systems for CO2 capture from flue gas, Int. J. Greenh. Gas Control. 53 (2016) 371–390, https://doi.org/10.1016/j.ijggc.2016.08.005.

[18] P.L. Mores, A.M. Arias, N.J. Scenna, M.C. Mussati, S.F. Mussati, Cost-based comparison of multi-stage membrane configurations for carbon capture from flue gas of power plants, Int. J. Greenh. Gas Control. 86 (2019) 177–190, https://doi.org/10.1016/j.ijggc.2019.04.021.

[19] S. Lee, M. Binns, J.K. Kim, Automated process design and optimization of membrane-based CO2 capture for a coal-based power plant, J. Membr. Sci. 563 (2018) 820–834, https://doi.org/10.1016/j.memsci.2018.06.057.

[20] R.W. Baker, B.T. Low, Gas separation membrane materials: a perspective, Macromolecules 47 (2014) 6999–7013, https://doi.org/10.1021/ma501488s.

[21] C. Ma, M. Wang, Z. Wang, M. Gao, J. Wang, Recent progress on thin film composite membranes for CO2 separation, J. CO2 Util. 42 (2020) 101296, https://doi.org/10.1016/j.jcou.2020.101296.

[22] L.S. White, K.D. Amo, T. Wu, T.C. Merkel, Extended field trials of Polaris sweep modules for carbon capture, J. Membr. Sci. 542 (2017) 217–225, https://doi.org/10.1016/j.memsci.2017.08.017.

[23] T.J. Kim, H. Vrålstad, M. Sandru, M.B. Hägg, Separation performance of PVAm composite membrane for CO2 capture at various pH levels, J. Membr. Sci. 428 (2013) 218–224, https://doi.org/10.1016/j.memsci.2012.10.009.

[24] Z. Qiao, S. Zhao, M. Sheng, J. Wang, S. Wang, Z. Wang, C. Zhong, M.D. Guiver, Metal-induced ordered microporous polymers for fabricating large-area gas separation membranes, Nat. Mater. 18 (2019) 163–168, https://doi.org/10.1038/s41563-018-0221-3.

[25] H. Liu, S. Dai, D.E. Jiang, Insights into CO2/N2 separation through nanoporous graphene from molecular dynamics, Nanoscale 5 (2013) 9984–9987, https://doi.org/10.1039/c3nr02852f.

[26] Z. Tian, S.M. Mahurin, S. Dai, D. en Jiang, Ion-gated gas separation through porous graphene, Nano Lett. 17 (2017) 1802–1807, https://doi.org/10.1021/acs.nanolett.6b05121.

[27] G. He, S. Huang, L.F. Villalobos, J. Zhao, M. Mensi, E. Oveisi, M. Rezaei, K. V. Agrawal, High-permeance polymer-functionalized single-layer graphene membranes that surpass the postcombustion carbon capture target, Energy Environ. Sci. 12 (2019) 3305–3312, https://doi.org/10.1039/c9ee01238a.

[28] L. Lin, H. Peng, Z. Liu, Synthesis challenges for graphene industry, Nat. Mater. 18 (2019) 520–524, https://doi.org/10.1038/s41563-019-0341-4.

[29] L. Giordano, D. Roizard, R. Bounaceur, E. Favre, Evaluating the effects of CO2 capture benchmarks on efficiency and costs of membrane systems for post-combustion capture: a parametric simulation study, Int. J. Greenh. Gas Control 63 (2017) 449–461, https://doi.org/10.1016/j.ijggc.2017.05.002.

[30] Y. Shindo, T. Hakuta, H. Yoshitome, Calculation methods for multicomponent gas separation by permeation, Separ. Sci. Technol. 20 (1985) 445–459, https://doi.org/10.1080/01496398508060692.

[31] F. Zhao, S.W. Zhang, F. Han, R. Da Li, Thermodynamics analysis of roots vacuum pump, J. Phys. Conf. Ser. 1519 (2020), https://doi.org/10.1088/1742-6596/1519/1/012016.

[32] S. Huang, J. He, X. Wang, G. Qiu, Theoretical model for the performance of liquid ring pump based on the actual operating cycle, Int. J. Rotating Mach. 2017 (2017), https://doi.org/10.1155/2017/3617321.

[33] E.S. Rubin, Understanding the pitfalls of CCS cost estimates, Int. J. Greenh. Gas Control 10 (2012) 181–190, https://doi.org/10.1016/j.ijggc.2012.06.004.

[34] R. Turton, R.C. Bailie, W.B. Whiting, J.A. Shaeiwitz, D. Bhattacharyya, Analysis, Synthesis, and Design of Chemical Processes, 1998, https://doi.org/10.5860/choice.36-0974.

[35] M. Scholz, T. Harlacher, T. Melin, M. Wessling, Modeling gas permeation by linking nonideal effects, Ind. Eng. Chem. Res. 52 (2013) 1079–1088, https://doi.org/10.1021/ie202689m.

[36] Z. Zhu, Y. Geng, D.W. Sun, Effects of operation processes and conditions on enhancing performances of vacuum cooling of foods: a review, Trends Food Sci. Technol. 85 (2019) 67–77, https://doi.org/10.1016/j.tifs.2018.12.011.

[37] A. Menon, V. Stojceska, S.A. Tassou, A systematic review on the recent advances of the energy efficiency improvements in non-conventional food drying technologies, Trends Food Sci. Technol. 100 (2020) 67–76, https://doi.org/10.1016/j.tifs.2020.03.014.

[38] V.R. Sagar, P. Suresh Kumar, Recent advances in drying and dehydration of fruits and vegetables: a review, J. Food Sci. Technol. 47 (2010) 15–26, https://doi.org/10.1007/s13197-010-0010-8.

[39] C.N. Cutter, Microbial control by packaging: a review, Crit. Rev. Food Sci. Nutr. 42 (2002) 151–161, https://doi.org/10.1080/10408690290825493.

[40] M.K. Kang, W.I. Lee, H.T. Hahn, Analysis of vacuum bag resin transfer molding process, Compos. Part A. 32 (2001) 1553–1560.

[41] F. Zhao, S. Zhang, K. Sun, Z. Zhang, Thermodynamic performance of multi-stage gradational lead screw vacuum pump, Appl. Surf. Sci. 432 (2018) 97–109, https://doi.org/10.1016/j.apsusc.2017.08.081.

[42] D. Collins, Choosing process vacuum pumps, Chem. Eng. Prog. 108 (2012) 65–72.

[43] L.M. Robeson, The upper bound revisited, J. Membr. Sci. 320 (2008) 390–400, https://doi.org/10.1016/j.memsci.2008.04.030.

[44] Envirowise, Cost-effective management of vacuum systems. http://www.wrap.org.uk/sites/files/wrap/GG101R_Final.pdf, 2008.

[45] D. Collins, CXS chemical dry vacuum pump brings smart vacuum to the process industry: edwards' next generation CXS pumps meet the industry's growing demands for highly reliable, highly flexible, quiet vacuum on demand, Vakuum Forsch. Praxis 24 (2012) 6–11, https://doi.org/10.1002/vipr.201200504.

[46] R.W. Baker, B. Freeman, J. Kniep, Y.I. Huang, T.C. Merkel, CO2 capture from cement plants and steel mills using membranes, Ind. Eng. Chem. Res. 57 (2018) 15963–15970, https://doi.org/10.1021/acs.iecr.8b02574.

[47] Eurostat, Electricity Prices for Non-household Consumers, 2019. https://ec.europa.eu/eurostat/statistics-explained/index.php/Electricity_price_statistics#Electricity_prices_for_non-household_consumers.

[48] R.W. Baker, Membrane Technology and Applications, 2012.

[49] G. He, Y. Mi, P.L. Yue, G. Chen, Theoretical study on concentration polarization in gas separation membrane processes, J. Membr. Sci. 153 (1999) 243–258, https://doi.org/10.4015/S1016237205000469.

[50] J. Catalano, M. Giacinti Baschetti, G.C. Sarti, Influence of the gas phase resistance on hydrogen flux through thin palladium-silver membranes, J. Membr. Sci. 339 (2009) 57–67, https://doi.org/10.1016/j.memsci.2009.04.032.

[51] Y. Han, W. Salim, K.K. Chen, D. Wu, W.S.W. Ho, Field trial of spiral-wound facilitated transport membrane module for CO2 capture from flue gas, J. Membr. Sci. 575 (2019) 242–251, https://doi.org/10.1016/j.memsci.2019.01.024.

[52] S. Huang, S. Li, L.F. Villalobos, M. Dakhchoune, M. Micari, D. Babu, M.T. Vahdat, M. Mensi, E. Oveisi, K.V. Agrawal, Millisecond lattice gasification for high-density CO_2- and O_2-sieving nanopores in single-layer graphene, Sci. Adv. 7 (2021) eabf0116. In press.